Physics of Fluids

A novel model for incorporation of differential diffusion effects in PDF simulations of non-premixed turbulent flames based on reaction-diffusion manifolds (REDIM)

Cite as: Phys. Fluids **33**, 025110 (2021); https://doi.org/10.1063/5.0039160
Submitted: 01 December 2020 • Accepted: 06 January 2021 • Published Online: 22 February 2021

Chunkan Yu (俞淳侃), Paola Breda, Felipe Minuzzi, et al.

COLLECTIONS

Paper published as part of the special topic on In Memory of Edward E. (Ted) Oâ€™Brien

This paper was selected as an Editor's Pick

View Online Export Citation CrossMark

ARTICLES YOU MAY BE INTERESTED IN

Experimental study of the effect of outlet boundary on combustion instabilities in premixed swirling flames
Physics of Fluids **33**, 027106 (2021); https://doi.org/10.1063/5.0038984

Three-dimensional spectral proper orthogonal decomposition analyses of the turbulent flow around a seal-vibrissa-shaped cylinder
Physics of Fluids **33**, 025106 (2021); https://doi.org/10.1063/5.0035789

A point-cloud deep learning framework for prediction of fluid flow fields on irregular geometries
Physics of Fluids **33**, 027104 (2021); https://doi.org/10.1063/5.0033376

© 2021 Author(s).

Physics of Fluids ARTICLE scitation.org/journal/phf

A novel model for incorporation of differential diffusion effects in PDF simulations of non-premixed turbulent flames based on reaction-diffusion manifolds (REDIM)

Cite as: Phys. Fluids 33, 025110 (2021); doi: 10.1063/5.0039160
Submitted: 1 December 2020 · Accepted: 6 January 2021 ·
Published Online: 22 February 2021

View Online Export Citation CrossMark

Chunkan Yu (俞淳侃),[1,a)] Paola Breda,[2] Felipe Minuzzi,[3] Michael Pfitzner,[2] and Ulrich Maas[1]

AFFILIATIONS

[1]Institute of Technical Thermodynamics, Karlsruhe Institute of Technology, Engelbert-Arnold-Strasse 4, 76131 Karlsruhe, Germany
[2]Institute of Thermodynamics, Bundeswehr University of Munich, Werner-Heisenberg-Weg 39, 85577 Neubiberg, Germany
[3]Instituto de Matemática e Estatística, Universidade Federal do Rio Grande do Sul, Av. Bento Gonçalves 9500, P. O. Box 15080, Porto Alegre, RS, Brazil

Note: This paper is part of the special topic, In Memory of Edward E. (Ted) Oâ-Brien.
[a)]**Author to whom correspondence should be addressed:** chunkan.yu@kit.edu

ABSTRACT

In this work, reaction-diffusion manifold (REDIM) reduced chemistry is used in the simulation of turbulent non-premixed flames based on a transported-*probability density function* model. Differential molecular diffusion is applied in the generation of the manifolds. This is the first work to consider the gradients of the reduced variables as additional parameters in the REDIM model, and one-directional gradients are utilized to generate the REDIM reduced chemistry. Hereby, the influence of turbulence on differential molecular diffusion is automatically considered in terms of reduced variable gradients, and the physical transport properties (e.g., diffusion coefficients) are used in a detailed way, without any additional modeling (e.g., unity-Lewis number assumption). Although the scalar gradients appear as multi-directional in a general turbulent reacting flow, previous direct numerical simulation analysis reveals that REDIMs generated from one-directional gradients can accurately describe the system featuring multi-directional gradients, if this one-directional gradient has a major effect on the chemistry. Here, it is proposed to obtain such gradients under the hypothesis that the flame structure is locally one-dimensional at each spatial position. In order to retrieve the gradients of the reduced variables for the interpolation of the thermo-kinetic states from the REDIM table, the sub-grid gradient is evaluated here from the particle fields. The well-known Sandia series of flames is selected to validate the proposed algorithm. The results show that the new algorithm can reproduce the thermo-kinetic quantities with high accuracy for all investigated flames.

© 2021 Author(s). All article content, except where otherwise noted, is licensed under a Creative Commons Attribution (CC BY) license (http://creativecommons.org/licenses/by/4.0/). https://doi.org/10.1063/5.0039160

I. INTRODUCTION

For a general reacting flow, the thermo-kinetic state with n_{sp} species is a set of scalars expressed as an $n = n_{sp} + 2$ dimensional vector $\Psi = (h, p, \phi_1, ..., \phi_{n_{sp}})^{\mathrm{T}}$, where h is the specific enthalpy, p the pressure and ϕ_i is the specific mole number of species i, defined as $\phi_i = w_i/M_i$ (w_i is the mass fraction and M_i the molar mass of species i). The evolution of the thermo-kinetic state due to chemical and transport processes can be described by the following partial differential equation (PDE) system:[1,2]

$$\frac{\partial}{\partial t}\Psi(\mathbf{x}, t) = \mathbf{F}(\Psi) - (\mathbf{u}\cdot\nabla)\Psi - \frac{1}{\rho}\nabla\cdot((\mathbf{D}\cdot\nabla)\Psi) = \Phi(\Psi). \quad (1)$$

Here, $\mathbf{u}$ is the velocity vector, $\mathbf{D}$ is the $n \times n-$ dimensional transport matrix, and ρ is the density. $\mathbf{F}$ is the n-dimensional source vector that accounts for the chemical reactions, which may involve hundreds of species depending on the fuel considered.[1–3] Therefore, the PDE system shows a high dimensionality. In addition, the numerical integration is slowed down by the stiffness of the governing equations due to the strongly non-linear dependence of the reaction rates on temperature and composition.[1–3] The problem of having both a high

dimensional and stiff PDE system leads the way for further development of chemistry reduction models.

The direct numerical simulations (DNSs) for both laminar and turbulent reacting flames reported in Ref. 4 show that only a part of the composition space is accessed. The thermo-kinetic states tend to approach common attracting manifolds after a short time and finally reach the equilibrium point. This is because the physical processes (e.g., convection and molecular diffusion) and the chemical reaction processes take place at time-scales differing by orders of magnitude.[1,2,5] Chemical time scales describe how fast each chemical mode relaxes to the equilibrium and cover a much wider range than the physical time-scales.[5] This observation leads to the development of low-dimensional manifold methods, where the chemical time-scales faster than the physical time-scales are decoupled from the system. Therefore, the system is only governed by the chemical time-scales comparable to or slower than the physical ones.[1,2,5] Thus, the system dynamics is governed by the m_s slowest modes ($m_s \ll n$) and the corresponding low-dimensional slow manifolds $\mathscr{M}$ are defined as

$$\mathscr{M} = \left\{\Psi : \Psi = \Psi(\Theta),\ \ \Psi : \mathbb{R}^{m_s} \rightarrow \mathbb{R}^{n}\right\}, \tag{2}$$

where Ψ is the state vector of the original full system. The reduced coordinates $\Theta = (\theta_1, \theta_2, ..., \theta_{m_s})^{\mathrm{T}}$ parametrize the slow manifold. Several chemistry reduction models based on the concept of low-dimensional attractors have been developed. Among them are the intrinsic low-dimensional manifold (ILDM),[5] the flame prolongation of ILDM (FPI),[6] the flamelet model,[7] the flamelet-generated manifold (FGM),[8] and the reaction-diffusion manifold (REDIM).[9] A review on this topic can be found, e.g., in Refs. 1 and 2. Such low-dimensional manifolds have the advantage of representing slow manifolds and the overall slow dynamics. The dimension of the governing equations can be therefore reduced through the use of manifold-based simplified chemistry.

Not only chemical kinetics but also molecular transport has an important influence on the thermo-kinetic states. To simplify the computational complexity without losing accuracy, many numerical calculations exploit the assumption of equal diffusivities (ED) (in particular, the case of unity Lewis numbers).[10–16] However, various experimental investigations such as Refs. 17–22 have reported the importance of differential molecular diffusion (DD) in turbulent reacting flows. Moreover, many numerical studies such as Refs. 23–29 confirm that an accurate prediction of species with high molecular diffusivity (e.g., H_2) or NOx and soot formation can only be achieved by using a detailed transport model including differential diffusion. This is because the molecular transport coefficients (matrix $\mathbf{D}$) are purely physical properties and do not depend on the external flow. In other words, with increasing turbulence intensity the transport processes will be enhanced, but the physical properties (e.g., transport coefficients) would remain unaffected.

Numerous methodologies have been developed to couple differential diffusion with detailed and reduced chemistry models, in particular for transported-*probability density function* (TPDF) simulations. One approach used in some works[30–33] is to introduce differential mixing timescales to describe the differential molecular diffusion in the mixing model. For example, in Ref. 30, an additional term is added to the standard mixing model parameter C_ϕ, to account for the enhancement of mixing by the differential molecular diffusion: $C_\phi^* = \alpha \cdot C_\phi$, where α is a model parameter depending on turbulent kinetic energy, turbulent dissipation, etc. In the context of flamelet modeling,[7] different approaches have been proposed. In Ref. 34, a new definition of mixture fraction is formulated for the flamelet equation[7] removing the previous assumption of equal diffusivity (unity Lewis number). In Ref. 35, the differential diffusion flamelet model is based on a combination of two flamelet libraries: one using the equal diffusivities transport model and the other using the differential molecular diffusion transport model. In Ref. 36, the non-unity Lewis number assumption is used in the near-injector zone and the unity Lewis number assumption further downstream. A manual switch between the models is made according to the reported experimental study. In Ref. 37, the REDIM chemistry is generated based on a detailed transport model to account for differential diffusion[38] in the transport matrix $\mathbf{D}$, while the effect of turbulence on the reduced chemistry is considered in terms of scalar dissipation rate. The latter becomes an additional progress variable. Other approaches accounting for differential diffusion in PDF models can be found in Refs. 39–42.

This work exploits the REDIM[9] as a reduced chemistry model. A detailed transport model[38] is applied to describe differential diffusion within the manifold. In the process of generating the REDIM, information about the scalar gradient is needed. In our previous work,[43–45] the scalar gradient was taken from steady laminar flame scenarios. However, such gradients in a turbulent flow can differ largely from those in a laminar flow. To take into account the influence of scalar gradients on the reduced chemistry, this work presents a novelty in the framework of the REDIM concept: the gradients of the reduced variables become progress variables. In other words, the selected reduced variables together with their gradients determine the thermo-kinetic states. However, scalar gradients in turbulent flows appear in a multi-directional way, so that the REDIM model with multi-directional gradients must be taken into consideration. This would complicate the computation because the corresponding REDIM model would be high dimensional. On the other hand, our previous work based on DNS analysis[46] shows that the REDIM model obtained from the one-directional gradient can accurately describe the system with multi-directional gradients, if this one-directional gradient contributes the major effect on the chemistry. In order to identify this major gradient component, the same idea as the flamelet concept[47] is used: the flame structure can be locally considered as one-dimensional. In other words, the species gradient in the flow field is dominated by a component in one major direction, which is normal to the flame surface. The previously investigated turbulent non-premixed flames, Sandia D–F[48] are selected as the reference case for this validation.

This work is organized as follows: Sec. II provides a short outline about the models used for the turbulence and the reduced chemistry. Section III introduces the *one-directional gradient approximation*. Section IV explains in detail the numerical procedure for the generation of the reduced chemistry and its coupling with models for turbulent flows. Finally, the validation of the proposed algorithm is shown in Sec. V. Important observations related to this investigation are summarized in the conclusions.

II. MATHEMATICAL MODELS

In the present work, the Reynolds-averaged Navier Stokes (RANS) equations coupled with the TPDF method are applied. In order to reduce the computational effort caused by detailed chemical kinetics (high dimension and high stiffness), the reaction-diffusion manifolds (REDIMs) reduced model is used. This section provides a brief overview for the methodology of each model.

© Author(s) 2021

A. Reynolds-averaged Navier Stokes (RANS) for the flow field

The governing conservation equations of this work are derived by applying Favre-averaging, namely, a quantity $f(\mathbf{x},t)$ is split into a Favre-averaged quantity $\widetilde{f}(\mathbf{x})$ and the corresponding Favre-fluctuation $f''(\mathbf{x},t)$: $f=\widetilde{f}+f''=\overline{\rho f}/\bar{\rho}+f''$. Thus, the Favre-averaged continuity equation and momentum equations for RANS can be written as

$$\frac{\partial\bar{\rho}}{\partial t}+\nabla\cdot(\bar{\rho}\widetilde{\mathbf{u}})=0, \tag{3}$$

$$\frac{\partial\bar{\rho}\widetilde{\mathbf{u}}}{\partial t}+\nabla\cdot(\bar{\rho}\widetilde{\mathbf{u}}\otimes\widetilde{\mathbf{u}})=-\nabla\bar{p}-\nabla\cdot\left(\bar{\rho}\mathbf{u}''\otimes\mathbf{u}''\right). \tag{4}$$

Here, t is the time and $\mathbf{u}=(u_1,u_2,u_3)^{\mathrm{T}}$ is the velocity vector. The symbol $\otimes$ is the dyadic product, and ∇ is the nabla operator $\nabla=(\frac{\partial}{\partial x_1},\frac{\partial}{\partial x_2},\frac{\partial}{\partial x_3})^{\mathrm{T}}$.

Note that, in the present work, the flow is considered as adiabatic, meaning that the total enthalpy is conserved for a low Mach number. Therefore, the conservation equation for energy is not needed in the CFD code, since the Favre-averaged temperature $\widetilde{T}$ is determined by the PDF, and the local values are retrieved from the reduced chemistry table (see Sec. II C). Equations (3) and (4) are closed by the Favre-averaged ideal gas equation: $\bar{p}=\bar{\rho}\cdot\widetilde{R_g T}$, where R_g is the mass-specific gas constant defined as $R_g=R/\bar{M}$ ($\bar{M}$: molar mass of mixture; $R=8.314\,\mathrm{J/(mol\,K)}$: universal gas constant). The unclosed Favre-averaged Reynolds stresses $\bar{\rho}\mathbf{u}''\otimes\mathbf{u}''$ are determined from the PDF part (see Sec. II B).

B. Transported-PDF (TPDF) model

The probability density function (PDF) method has been developed for several decades and applied to a wide class of flows. The TPDF equation derived by Dopazo and O'Brien[49–51] and Pope[52] shows a remarkable advantage: chemical reactions can be treated in an exact way, without approximation. In the present work, a joint PDF of velocity-composition-turbulent frequency (VCF-PDF) is employed.[53,54] This joint PDF is a one-point, one time PDF consisting of three components: the velocity $\mathbf{u}$, the n-dimensional thermo-kinetic states Ψ, and the turbulent frequency ω. A TPDF equation for this VCF-PDF can be derived,[52,53] and it shows the main advantage of PDF methods, i.e., the chemical reaction term does not require any modeling.[52,55] The derived TPDF equation can be solved numerically by using the Monte Carlo particle method,[52] where the PDF is represented by an ensemble of notional particles with flow and thermo-kinetic properties (position $\mathbf{x}^*$, velocity fluctuation $\mathbf{u}''^{,*}$, thermo-kinetic states Ψ^*, and turbulent frequency ω^*) evolving according to stochastic processes.[52,55]

The evolution of the notional particle properties is described by the following stochastic differential equations (SDEs):[52,54,56]

$$\mathrm{d}\mathbf{x}^*=(\widetilde{\mathbf{u}}+\mathbf{u}''^{,*})\mathrm{d}t, \tag{5a}$$

$$\mathrm{d}\mathbf{u}''^{,*}=\frac{1}{\bar{\rho}}\nabla\cdot\left(\bar{\rho}\mathbf{u}''\otimes\mathbf{u}''\right)\mathrm{d}t-(\mathbf{u}''^{,*}\cdot\nabla)\widetilde{\mathbf{u}}-\left(\frac{1}{2}+\frac{3}{4}C_0\right)\Omega\mathbf{u}''^{,*}\mathrm{d}t+\sqrt{C_0 k\Omega}\cdot\mathrm{d}\mathbf{W}, \tag{5b}$$

$$\mathrm{d}\omega^*=-C_3\Omega(\omega^*-\widetilde{\omega})\mathrm{d}t-S_\omega\Omega\omega^*\mathrm{d}t+\sqrt{2C_3C_4\Omega\widetilde{\omega}\omega^*}\cdot\mathrm{d}W, \tag{5c}$$

$$\mathrm{d}\Psi^*=\mathbf{F}(\Psi^*)\cdot\mathrm{d}t+\mathbf{M}\cdot\mathrm{d}t, \tag{5d}$$

where S_ω is the sink of turbulent frequency

$$S_\omega=C_{\omega2}-C_{\omega1}\cdot\frac{\mathscr{P}}{k\cdot\Omega}, \tag{6}$$

$\mathscr{P}$ is the turbulence production, k is the turbulent kinetic energy, and Ω is the conditionally averaged turbulent frequency:

$$\mathscr{P}=\mathbf{u}''\otimes\mathbf{u}'':\nabla\widetilde{\mathbf{u}}=-\widetilde{u_i''u_j''}\cdot\frac{\partial\widetilde{u}_i}{x_j}, \tag{7a}$$

$$k=\frac{1}{2}\widetilde{\mathbf{u}''\cdot\mathbf{u}''}=\frac{1}{2}\widetilde{u_i''u_i''}, \tag{7b}$$

$$\Omega=C_\Omega\cdot\frac{\overline{\rho^*\omega^*|\omega^*\geq\widetilde{\omega}}}{\bar{\rho}}. \tag{7c}$$

All values for the model parameters C_0, C_Ω, $C_{\omega1}$, $C_{\omega2}$, C_3, C_4, and C_ϕ used in the simulation in the present work will be listed later. In Eq. (5d), the terms $\mathbf{F}(\Psi^*)$ and $\mathbf{M}$ are, respectively, the source term of the thermo-kinetic states and the mixing process. The modeling of the mixing process in the framework of PDF methods plays an important role for the simulation accuracy. The simplest mixing model is the interaction by exchange with the mean (IEM) developed by Dopazo and O'Brien,[57] which is expressed as

$$\mathbf{M}=-\frac{1}{2}\cdot C_\phi\cdot(\Psi^*-\widetilde{\Psi})\Omega. \tag{8}$$

However, the IEM model has the main drawback: the shape of the scalar PDF remains unchanged; thus, it does not relax to a Gaussian distribution.[55,58] Many other models satisfying this requirement are therefore developed, such as the Euclidean minimum spanning trees (EMST),[59] the multiple mapping conditioning (MMC),[60] or the parameterized scalar profiles (PSP).[61] References 58 and 62 provide a detailed review about the mixing models available in the literature.

C. Reaction-diffusion manifolds (REDIMs) for reduced chemistry

The reaction-diffusion manifolds (REDIMs)[9] used in this work identify the low-dimensional invariant manifold $\mathscr{M}$ [cf. Eq. (2)], which accounts for physical transport. The REDIM can be obtained by solving the following evolution equation toward the steady solution:[9]

$$\frac{\partial\Psi(\Theta)}{\partial t}=\left(\mathbf{I}-\Psi_\Theta(\Theta)\cdot\Psi_\Theta^+(\Theta)\right)\cdot\left\{\mathbf{F}(\Psi(\Theta))-\frac{1}{\rho}\left[(\mathbf{D}\Psi_\Theta\cdot\chi(\Theta))_\Theta\cdot\chi(\Theta)\right]\right\}, \tag{9}$$

where Ψ_Θ is the matrix of partial derivatives of Ψ with respect to Θ ($(\Psi_\Theta)_{i,j}=\partial\psi_i/\partial\theta_j$). Ψ_Θ^+ is the Moore–Penrose pseudo-inverse of Ψ_Θ. In addition, $\chi(\Theta)$ is the gradient estimate expressed as

© Author(s) 2021

$$\chi(\Theta) = \nabla\Theta = \begin{bmatrix} | & | & & | \\ \nabla\theta_1 & \nabla\theta_2 & \cdots & \nabla\theta_{m_s} \\ | & | & & | \end{bmatrix}^{\mathrm{T}} = \begin{bmatrix} \frac{\partial\theta_1}{\partial x_1} & \frac{\partial\theta_2}{\partial x_1} & \cdots & \frac{\partial\theta_{m_s}}{\partial x_1} \\ \frac{\partial\theta_1}{\partial x_2} & \frac{\partial\theta_2}{\partial x_2} & \cdots & \frac{\partial\theta_{m_s}}{\partial x_2} \\ \frac{\partial\theta_1}{\partial x_3} & \frac{\partial\theta_2}{\partial x_3} & \cdots & \frac{\partial\theta_{m_s}}{\partial x_3} \end{bmatrix}^{\mathrm{T}}, \tag{10}$$

where $\mathbf{x} = (x_1, x_2, x_3)^{\mathrm{T}}$ is the vector of the spatial coordinates. The use of Eq. (9) to generate the REDIM is linked to several advantages compared to other manifold methods:

- There is no restriction to the dimensions of the reduced chemistry. In other words, reduced chemistry with arbitrary dimensions for the reduced coordinate vector Θ can be constructed.[63]
- Differential molecular diffusion can be implemented through the transport matrix $\mathbf{D}$ in Eq. (9), accounting for the transport properties and their influence onto the thermo-kinetic state space of the reduced system.[64]
- If the gradients for the investigated turbulent flow are available (e.g. from DNS data), then a multi-directional gradient estimate can be supplied to generate the REDIM reduced chemistry.[46]
- The effect of gradients on the reduced system can be included in the model through the estimate $\chi(\Theta)$ in Eq. (9) (see Sec. IV A). This corresponds to taking into account the stronger gradients observed for turbulent flows.
- As shown in Ref. 65, the REDIM evolution equation Eq. (9) is invariant with respect to a change of the reduced coordinates, as long as uniqueness of the mapping is guaranteed. Thus, the REDIM method allows a simple analysis of the hierarchy of manifolds of different dimensions.[65]

A critical point to understand here is that the gradient estimate $\chi(\Theta)$ must be provided for the generation of REDIMs in Eq. (9). Different approaches have already been applied in our previous papers:

- The gradient can be estimated by representative constant values along the manifold, namely, $\chi(\theta) = \text{const.}$[43] However, this assumption may be inaccurate because scalar gradients can vary largely depending on the flow Reynolds number.[66,67]
- The gradients can be taken from typical flame scenarios including burning flames and pure mixing processes as well as extinction and ignition processes.[44,45,68–70] Usually, a set of flamelets has to be chosen. If premixed flames are involved, the turbulence will hardly change the scalar gradients in the reaction zone.[71,72] In this case, gradients obtained from flames appear as a reasonable choice for the generation of the REDIM. However, the scalar gradients from turbulent non-premixed flames can be considerably different from those found in laminar flames,[73] which could lead to modeling errors.
- The gradients can be taken from DNS data whenever available.[46] This is the most accurate way to include the real behavior of the investigated combustion system, but it is computationally expensive.

A common property to these different approaches is that the system scalar gradients are assigned to the REDIM evolution equation (9) as *a priori* information, before the reduced chemistry is stored in a database. However, scalar gradients depend strongly on the instantaneous flow field (e.g., local Reynolds number, turbulent frequency, etc.) and change in time and space.[74–76]

There are two different strategies to overcome the limitation derived by the gradient guess. One possibility is to increase the dimensions of the REDIM reduced chemistry (the number of reduced variables θ) because the gradient estimate becomes less and less important with increasing dimensions.[9,63] The other strategy, used in the present work, is to consider the scalar gradients as additional variables in the REDIM chemistry. In this case, the REDIM reduced chemistry is defined as

$$\mathcal{M} = \left\{\Psi : \Psi = \Psi(\Theta, \chi(\Theta)),\ \ \Psi : \mathbb{R}^{4m_s} \rightarrow \mathbb{R}^n\right\}. \tag{11}$$

The dimension is now $4m_s$, because for each reduced coordinate its gradient generally points in three directions. If one only considers the gradient in one direction, which we will call the one-directional gradient, Eq. (9) can be simplified to the following expression:

$$\frac{\partial\Psi(\Theta)}{\partial t} = \left(\mathbf{I} - \Psi_\Theta(\Theta)\cdot\Psi_\Theta^{+}(\Theta)\right) \cdot\left\{\mathbf{F}(\Psi(\Theta)) - \frac{1}{\rho}\left[\left(\mathbf{D}\Psi_\Theta\cdot\hat{\chi}(\Theta)\right)_\Theta\cdot\hat{\chi}(\Theta)\right]\right\}, \tag{12}$$

with

$$\hat{\chi}(\Theta) = \left[\frac{\partial\theta_1}{\partial z}\ \ \frac{\partial\theta_2}{\partial z}\ \ \cdots\ \ \frac{\partial\theta_{m_s}}{\partial z}\right]^{\mathrm{T}}, \tag{13}$$

and $\mathbf{D}$ the same $n\times n$-dimensional transport matrix as in Eq. (1). Here, the REDIM manifold based on one-directional gradients is stored as

$$\mathcal{M} = \left\{\Psi : \Psi = \Psi(\Theta, \hat{\chi}(\Theta)),\ \ \Psi : \mathbb{R}^{2m_s} \rightarrow \mathbb{R}^n\right\}. \tag{14}$$

Figure 1 shows the influence of the gradient estimate for a one-dimensional REDIM for counterflow diffusion flames with $\theta = \mathrm{N}_2$ (in specific mole numbers) and a one-directional gradient, and the physical transport properties are determined in a detailed way. It is observed clearly that with different gradients, one obtains different REDIM models. If the gradient $\hat{\chi}(\theta)$ increases to a certain value [here in this example $\hat{\chi}(\theta) = 3000$], the REDIM provides an extinguished solution. This can be understood as follows: if the scalar dissipation rate becomes larger, the Damköhler-number (ratio of the physical transport and chemical time scales) becomes smaller, so that chemical reactions cannot take place since the fresh reactants are removed quicker than the reaction requires. An extinguished solution is therefore obtained. In this example, the REDIM reduced chemistry is written as $\mathcal{M} = \left\{\Psi : \Psi = \Psi(\mathrm{N}_2, \hat{\chi}(\mathrm{N}_2)),\ \ \Psi : \mathbb{R}^2 \rightarrow \mathbb{R}^n\right\}$. Clearly, the influence of scalar gradients on the chemistry can be potentially well captured in the concept of REDIMs automatically.

It must be emphasized again that the influence of scalar gradients on the REDIM model becomes less and less important with increasing the dimension of the REDIM model. For low dimensions (say less than or equal to two dimensions) of the REDIM model, the scalar gradients play an important role, while the scalar gradients play a minor

© Author(s) 2021

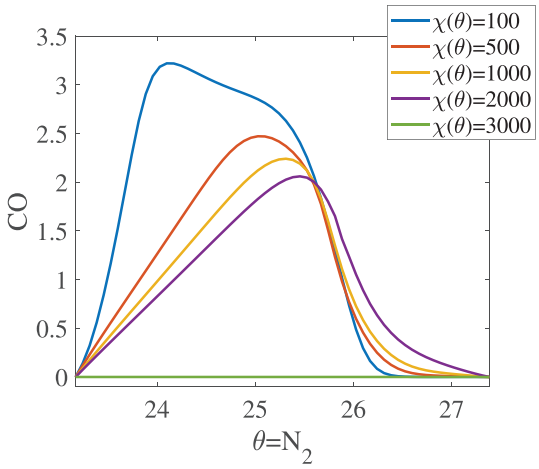

FIG. 1. Example of influence of gradient estimate $\chi(\theta)$ using a one-dimensional REDIM.

role for high dimensions (say larger than three dimensions), which have already shown in our previous work such as in Refs. 9, 63, and 77.

The advantage of including the gradients as additional independent variables in the REDIM model is that depending upon different gradients $\chi(\Theta)$, one obtains different REDIM models. Furthermore, the gradients are related closely to the turbulence intensity in the flow field. Therefore, the influence of scalar gradients on the change of the chemical states is taken into account directly via the REDIM model, and no additional models for the physical transport properties are needed (e.g., unity-Lewis number assumption or introduction of turbulent diffusivity[30]).

In fact, the gradients can be easily calculated from DNS. However, in a general three-dimensional flow, the scalar gradients are three directional and the corresponding REDIM reduced model of Eq. (11) has high dimensions [e.g., Eq. (8), if two reduced variables are considered]. In contrast, the REDIM model generated using one-directional gradients of Eq. (14) is more computational efficient in its application, because one obtains a four-dimensional REDIM model using two reduced variables. Here, we propose an approximation to justify the use of a one-directional gradient REDIM for a multidimensional flow. This approximation is similar to the idea of the flamelet concept that the flame structure can be locally considered as one-dimensional and depends only on the coordinate normal to some *iso*-surface describing the flame structure.[47,78] This concept will be discussed in detail in Sec. III.

III. ONE-DIRECTIONAL GRADIENT APPROXIMATION FOR THE TURBULENT REACTING FLOWS

In general, the gradient estimate for the $k-$ th reduced variable in turbulent reacting flows must be expressed as a vector of multi-directional gradient in the REDIM concept as well [cf. Eq. (10)]

$$\chi(\theta_k) = \nabla\theta_k = \nabla_{\mathbf{e}_1}\theta_k \cdot \mathbf{e}_1 + \nabla_{\mathbf{e}_2}\theta_k \cdot \mathbf{e}_2 + \nabla_{\mathbf{e}_3}\theta_k \cdot \mathbf{e}_3, \tag{15}$$

where $\mathbf{e}_i$ ($i = 1$, 2, and 3) is the element in the basis unity vectors of the spatial space, and $\nabla_{\mathbf{e}_i}\theta_k$ is the directional derivative of gradient $\nabla\theta_k$ in direction $\mathbf{e}_i$

$$\nabla_{\mathbf{e}_i}\theta_k = \nabla\theta_k \cdot \mathbf{e}_i. \tag{16}$$

On the one hand, using this multi-directional gradient is the most accurate way to capture the effect of the gradients on the chemistry. On the other hand, it results in a high-dimensional REDIM reduced chemistry. The computational efficiency is considerably reduced.

To overcome this difficulty, Schiessl *et al.*[46] studied the effect of gradients on the chemistry based on the DNS analysis. In their analysis, the multi-directional gradient was taken from a DNS database and decomposed into three directions using a singular vector decomposition, so that the first term in Eq. (15) represents the major contribution to the REDIM model. This term was closely related to a one-dimensional flame structure, which is typically assumed in the flamelet context.[47] The remaining terms in Eq. (15) are considered as a correction for the one-dimensional flame structure assumption. This allowed to account for the effect of the multi-directional gradient in turbulent flames on the REDIM model. Under such circumstances, the REDIM obtained from the gradient part sharing the major contribution ($\nabla_{\mathbf{e}_1}\theta_k \cdot \mathbf{e}_1$) can be used to accurately describe a system with multi-directional gradients. Alternatively said, the REDIM model can be generated by using a one-dimensional gradient Eq. (12), and the manifold is stored according to $\Psi = \Psi(\Theta, \hat{\chi}(\Theta))$, and the gradient part with the major contribution will be used at run-time to retrieve the thermo-kinetic states from the table.

The remaining question is how to identify the gradient with the major contribution on chemistry, using the information from the flow fields. To solve this problem, we begin with a general description of turbulent non-premixed reacting flows, as represented in Fig. 2. Although a two-dimensional flow is shown, the discussion can be straightforwardly extended to a three-dimensional flow. Depending on the turbulence intensity, the flame (gray surface) can appear as strongly distorted or even fragmented.[47,78–80] However, for non-premixed flames, one can easily determine the *iso*-surface for the mixture fraction ξ (*iso*-ξ-surface in figure). The normal vector of *iso*-ξ-surface $\mathbf{n}_\xi$ (black arrow) can be easily obtained from

$$\mathbf{n}_\xi = -\frac{\nabla\xi}{|\nabla\xi|}, \tag{17}$$

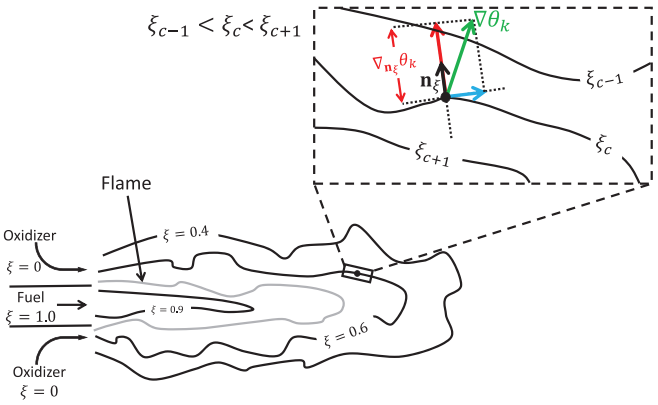

FIG. 2. Schematic representation of the proposed algorithm for general turbulent condition.

© Author(s) 2021

where $|\cdot|$ is the Euclidean norm. Afterwards the $\mathbf{n}_\xi^\perp$ which satisfies $\mathbf{n}_\xi^\perp \cdot \mathbf{n}_\xi = 0$ determines the basis vector for the *iso*-ξ-surface.

The introduction of the *iso*-ξ-surface and its normal vector $\mathbf{n}_\xi$ allows treating the flame structure similarly to the flamelet concept;[47] although the flow is multi-dimensional, one can consider the flame structure locally as a one-dimensional structure. Under this hypothesis, it is assumed that the reduced variable gradient in the direction normal to the *iso*-ξ-surface ($\nabla_{\mathbf{n}_\xi}\theta_k$, red arrow in Fig. 2) can be considered as the gradient part having major contribution on the reduced chemistry. The contribution along the *iso*-ξ-surface instead (blue arrow in Fig. 2) has a minor effect on the chemistry and is therefore neglected. In this way, we write the reduced variable gradient along direction $\mathbf{n}_\xi$ as

$$|\nabla\theta_k| \approx \nabla_{\mathbf{n}_\xi}\theta_k = \nabla\theta_k \cdot \mathbf{n}_\xi. \tag{18}$$

IV. NUMERICAL PROCEDURE

A. Generation of REDIM reduced chemistry

To illustrate the generation of the reduced chemistry, the counterflow diffusion flame configuration corresponding to the Sandia flame[48] inlet conditions is considered:

- Fuel side: main jet having a mixture composition of 25% methane + 75% air by volume, $p = 1$ bar, and $T = 294$ K.
- Oxidizer side: co-flow having mixture composition of 100% air, $p = 1$ bar, and $T = 292$ K.

The numerical simulations for the detailed calculation and generation of the REDIM model are performed using the in-house HOMREA and INSFLA code.[81] The molecular transport model is based on Curtiss–Hirschfelder approximation,[38] and it includes the Soret effect[82] (note that more complex models can be handled). The mixture fraction is defined consistently with the definition provided for experimental measurements[48]

$$\xi = \frac{2(w_C - w_{C,2})/M_C + 0.5(w_H - w_{H,2})/M_H}{2(w_{C,1} - w_{C,2})/M_C + 0.5(w_{H,1} - w_{H,2})/M_H}, \tag{19}$$

where w_C and w_H are the elemental mass fractions of C and H, M_C and M_H the atomic weights. The subscript 1 refers to the fuel side (main jet), and subscript 0 to the oxidizer side (co-flow air). A detailed description of the REDIM generation procedure can be found in the literature in Refs. 44, 45, and 63. Hereby, only the important issues related to the numerical procedure will be addressed.

Figure 3 shows the REDIM reduced chemistry projected onto the N_2-CO_2 space. To solve the REDIM evolution equation (12), the boundary conditions enclosing the application range of the reduced chemistry should be defined first. The upper boundary is defined using the Burke–Schumann solution[83] since the system is considered as adiabatic, while the lower boundary is a pure mixing line without reactions. Such boundaries include all possible flame scenarios, namely, stable flames with different strain rates and the extinction regime. The initial condition for the numerical integration of Eq. (12) can be chosen arbitrarily, since only the stationary solution of Eq. (12) is of interest. Before integrating the REDIM evolution equation (12), the reduced coordinate system Θ shall be defined. In Refs. 84–87, it was shown that a two-dimensional REDIM is sufficient to describe the Sandia flames D and E, while for the Sandia flame F a three-dimensional REDIM should be considered to increase the accuracy.[87] In this work, the investigation is limited to REDIMs based on two reduced variables (θ_1, θ_2) because we improve the accuracy by taking into account the varying gradients. Thus, the REDIM manifold for the simulation of Sandia flames is finally represented by

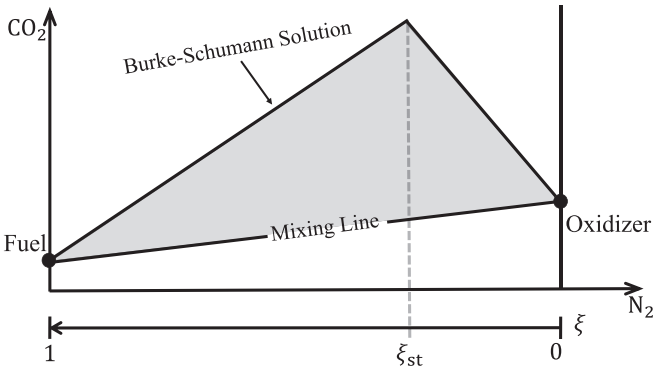

FIG. 3. Schematic representation of generation of REDIM reduced chemistry.

$$\mathscr{M} = \left\{\Psi : \Psi = \Psi(\theta_1, \theta_2, \hat{\chi}(\theta_1), \hat{\chi}(\theta_2)), \quad \Psi : \mathbb{R}^4 \rightarrow \mathbb{R}^n\right\} \tag{20}$$

and it will be labeled as REDIM-grad throughout the whole work. Note that although two reduced variables (θ_1, θ_2) are used, the REDIM-grad reduced chemistry is four-dimensional.

B. Application of REDIM reduced chemistry in the PDF particle method

In the context of REDIM, as well as in many other tabulated chemistry models, all information related to thermo-kinetic states such as enthalpy, species concentrations, and their thermo-kinetic source terms can be stored as functions of reduced coordinates. If the instantaneous values of the reduced coordinates are known, all other thermo-kinetic values can be extracted from the REDIM table. Therefore, instead of the full thermo-kinetic state Ψ^*, the notional particles in the PDF particle method carry thermo-kinetic information in terms of reduced coordinates Θ^*. The evolution of such coordinates due to reaction and mixing using the IEM model[57] yields an equation similar to Eq. (5d)

$$\mathrm{d}\Theta^* = \mathbf{F}(\Theta^*, \hat{\chi}(\Theta^*)) \cdot \mathrm{d}t + \mathbf{M} \cdot \mathrm{d}t. \tag{21}$$

Here, the mixing processes $\mathbf{M}$ take place directly in the reduced coordinate space. For example in the IEM, the mixing process based on reduced coordinates is written as

$$\mathbf{M} = -\frac{1}{2} \cdot C_\phi \cdot (\Theta^* - \widetilde{\Theta})\Omega. \tag{22}$$

The reaction processes $\mathbf{F}$ are interpolated from the REDIM table using the calculated values of Θ^* and $\hat{\chi}(\Theta^*)$.

While the values of Θ^* can be easily obtained from the instantaneous notional particle properties, the gradients $\hat{\chi}(\Theta^*)$ must be determined at each evolution step. Various strategies to define the gradient of the $k-$ th reduced variable θ_k^* can be considered:

© Author(s) 2021

- In the first variant, one can set the $\hat{\chi}(\theta_k^*)$ to be the real sub-grid gradient of θ_k^{FV} for each finite-volume (FV) cell in $\mathbf{n}_\xi$ direction: $\hat{\chi}(\theta_k^*) = \nabla_{\mathbf{n}_\xi}\theta_k{}^{\mathrm{FV}} = \nabla_{\mathbf{n}_\xi}\widetilde{\theta}_k{}^{\mathrm{FV}} + \nabla_{\mathbf{n}_\xi}\theta_k''{}^{,\mathrm{FV}}$, where $\theta_k''{}^{,\mathrm{FV}}$ is the fluctuation gradient and $\widetilde{\theta}_k{}^{\mathrm{FV}}$ is the weighted mean value of θ_k^* from all notional particles N_p

$$\widetilde{\theta}_k{}^{\mathrm{FV}} = \frac{\sum_{i=1}^{N_p} m^{*,i}\cdot\theta_k^{*,i}}{\sum_{i=1}^{N_p} m^{*,i}}, \quad \text{for one FV cell} \tag{23}$$

  with m^* being the notional particle mass. The calculation of $\theta_k''{}^{,\mathrm{FV}}$ is not straightforward, because it requires an additional transport equation.[88–90] The computational cost is therefore increased.
- In the second variant, one can set the $\hat{\chi}(\theta_k^*)$ to be the gradient of $\widetilde{\theta}_k{}^{\mathrm{FV}}$ for each finite-volume (FV) cell in $\mathbf{n}_\xi$ direction: $\hat{\chi}(\theta_k^*) = \nabla_{\mathbf{n}_\xi}\widetilde{\theta}_k{}^{\mathrm{FV}}$. Although this strategy is simple, it ignores the effect of turbulent fluctuations on the scalar gradients, thus $\nabla_{\mathbf{n}_\xi}\theta_k''{}^{,\mathrm{FV}} = 0$.
- The third variant, followed in this work, is to assume that the real sub-grid gradients can be approximated (at least as a coarse approximation) by gradients evaluated from the particle field. $\hat{\chi}(\theta_k^*)$ must be calculated for each notional particle depending on its instantaneous spatial position and the value retrieved from its neighbors, namely,

$$\hat{\chi}(\theta_k^*) = \nabla_{\mathbf{n}_\xi^*}\theta_k^* = \nabla\theta_k^*\cdot\mathbf{n}_\xi^*, \tag{24}$$

  where

$$\mathbf{n}_\xi^* = -\frac{\nabla\xi^*}{|\nabla\xi^*|}. \tag{25}$$

  The numerical implementation to calculate the scalar gradient from the particle field will be discussed in Sec. IV C. It shall be mentioned here that the real sub-grid gradients represented by the gradients evaluated from the particle field are only an estimate. Numerical simulations show that this approximation largely depends on the number of notional particles and the CFD cell size (see Sec. V A). By increasing the number of notional particles per CFD cell and reducing the cell size, this approximation gives reasonably good results.

C. Numerical implementation

Figure 4 summarizes the whole numerical procedure. In the RANS model, the Favre-averaged continuity and momentum equations (3) and (4) are solved to obtain the Favre-averaged density $\bar{\rho}^{\mathrm{FV}}$ and velocity $\tilde{\mathbf{u}}^{\mathrm{FV}}$ for each CFD cell, which are fed into the code of the PDF particle method. A certain amount of notional particles N_p is contained in each cell. For each notional particle, the evolution of the spatial position $\mathbf{x}^*$ is calculated using Eq. (5a), the evolution of the velocity fluctuations $\mathbf{u}''^{,*}$ using Eq. (5b), the evolution of the turbulent frequency ω^* using Eq. (5c), and the evolution of the reduced coordinates $\boldsymbol{\Theta}^*$ using Eq. (21).

In the last step, the values of the reduced coordinates for each notional particle together with the particle position in space are fed into the REDIM code, in order to retrieve the thermo-kinetic source terms. The gradients of the reduced variables shown in Eq. (24) are calculated numerically at run-time using a finite difference method (FD). For the $k-$ th reduced variable θ_k^* in a two-dimensional domain, the differentiation becomes

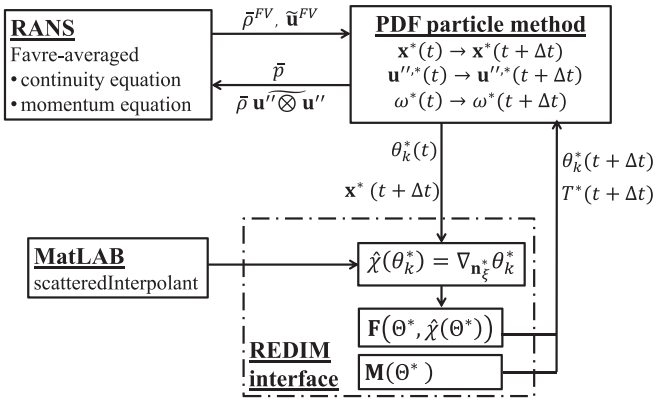

FIG. 4. Flow chart for the hybrid FVM/TPDF method coupled with REDIM reduced chemistry.

$$\nabla\theta_k^* = \begin{pmatrix} \left.\frac{\partial\theta_k^*}{\partial x_1}\right|_{x_2} \\ \left.\frac{\partial\theta_k^*}{\partial x_2}\right|_{x_1} \end{pmatrix} = \begin{pmatrix} \frac{\theta_k^*(x_1+\Delta x_1,x_2)-\theta_k^*(x_1-\Delta x_1,x_2)}{2\Delta x_1} \\ \frac{\theta_k^*(x_1,x_2+\Delta x_2)-\theta_k^*(x_1,x_2-\Delta x_2)}{2\Delta x_2} \end{pmatrix}. \tag{26}$$

To obtain the values at positions $\theta_k^*(x_1\pm\Delta x_1, x_2\pm\Delta x_2)$, the built-in function *scatteredInterpolant()* of MATLAB *version R2020a*[91] is used, which performs an interpolation on a 2D dataset based on the Delaunay triangulation algorithm.[92] The values $\theta_k^*(x_1\pm\Delta x_1, x_2\pm\Delta x_2)$ are affected by the neighbor particles of $\theta_k^*(x_1,x_2)$ as shown in Fig. 5. According to this figure, all the particles in the same cell (C) and the ones in the neighbor cells (NW, N, NE, W, E, SW, S, and SE) are selected for the interpolation of the values $\theta_k^*(x_1\pm\Delta x_1, x_2\pm\Delta x_2)$. The input vector passed to the function *scatteredInterpolant()* contains the positions of all selected particles $\mathbf{X}_1$ for the x_1- coordinate and $\mathbf{X}_2$ for the x_2- coordinate, as well as the $k-$ th reduced variable of all selected particles in the column vector $\boldsymbol{\Theta}_k$. The MATLAB function $\mathscr{F} = scatteredInterpolant(\mathbf{X}_1, \mathbf{X}_2, \boldsymbol{\Theta}_k)$ creates an interpolant that fits a surface of the form $\theta_k = \mathrm{F}(x_1,x_2)$ (blue surface in Fig. 5). From there, one can calculate the interpolated values as $\theta_k^*(x_1\pm\Delta x_1, x_2\pm\Delta x_2) = \mathscr{F}(x_1\pm\Delta x_1, x_2\pm\Delta x_2)$. Note that the proposed algorithm to calculate the gradient for each particle can also be extended to the 3D case, and the function *scatteredInterpolant()* of MATLAB *version R2020a*[91] can be directly applied for a 3D dataset.

The source term can be therefore interpolated based on the information of $\boldsymbol{\Theta}^*$ and $\hat{\chi}(\boldsymbol{\Theta}^*)$. Once the thermo-kinetic source term $\mathbf{F}(\boldsymbol{\Theta}^*, \hat{\chi}(\boldsymbol{\Theta}^*))$ and the mixing term $\mathbf{M}(\boldsymbol{\Theta}^*)$ are calculated, they are fed back to the PDF particle module. The temperature of each particle is also retrieved from table lookup. Particles belonging to the same CFD cell are used to calculate the Favre-averaged temperature $\widetilde{R_g T}$, with R_g being the gas constant.

© Author(s) 2021

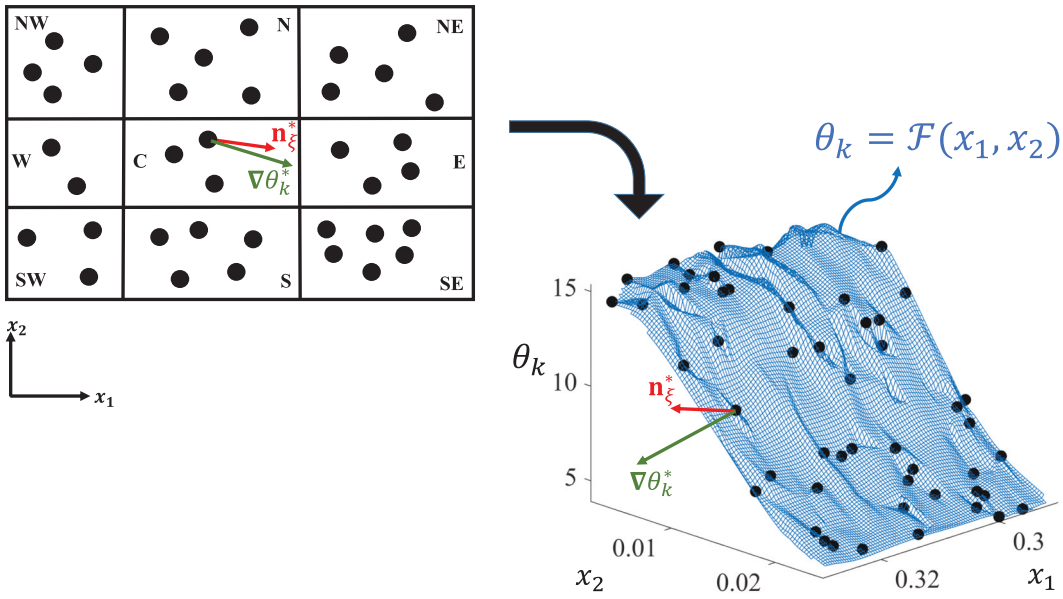

FIG. 5. Schematic representation of gradient determination of notional particles in 2D spatial coordinates.

Finally, the averaged pressure for each computational cell is determined as

$$\bar{p} = \bar{\rho} \cdot \widetilde{R_g T}, \tag{27}$$

and it is supplied back to RANS module.

D. Summary of the proposed methodology

Before discussing the validation results, we summarize hereby the proposed methodology. The numerical simulation is performed using the hybrid RANS/TPDF model coupled with the REDIM reduced chemistry. The REDIM model used in this work, labeled as REDIM-grad, is parametrized by the reduced coordinates Θ and their one-directional gradients $\hat{\chi}(\Theta)$. The values of the gradients supplied for the REDIM-grad table are derived from two assumptions:

- A previous analysis of DNS data showed that the scalar gradients are dominated by a component in one major direction, which has a main effect on the reduced chemistry. Information of the thermo-kinetic states retrieved from the REDIM-grad using this major component is the same of a system including multi-directional gradients. The first assumption (discussed in Sec. III) states that the flame structure can be locally considered as one-dimensional, as typically assumed in the flamelet concept.[47] The major component of the scalar gradients is the component belonging to the normal *iso*-ξ-surface, thus pointing along direction $\mathbf{n}_\xi$. This assumption is valid if the gradient of the reduced variables is almost aligned with $\mathbf{n}_\xi$. In other words, the component along the tangential space to the *iso*-ξ-surface remains negligibly small.
- The second assumption (discussed in Sec. IV B) states that the sub-grid gradients are approximated by the gradients in the fields represented by the notional particles. This is a strong assumption, and its accuracy depends largely on the number of notional particles used on a single computational cell (the discussion follows in Sec. V).

V. RESULTS AND DISCUSSION

To validate the proposed methodology, the well-known methane/air piloted turbulent jet flames (Sandia flames D–F[48]) are used as experimental test-case. This flame series is of great interest because with increasing jet velocity (Reynolds numbers: $\mathrm{Re_D} = 22\,400$, $\mathrm{Re_E} = 33\,600$, and $\mathrm{Re_F} = 44\,800$) the scalar gradients vary significantly[75,93] and their influence on (reduced) chemical kinetics is worth to be investigated. Furthermore, species such as H_2, which is also experimentally measured, need to be well predicted to capture the effect of differential molecular diffusion.

The computational domain and numerical parameters are consistent with those used in our previous works Refs. 85–87. Simulations are run on a 120 $D_j \times$ 40D_j domain ($D_j = 7.2$ mm is the diameter of the main jet pipe), discretized on a non-uniform grid of 51 × 42 CFD cells (for a total of 2142 cells). The numerical parameters and their values for each model used in the TPDF method are listed in Table I. The EMST mixing model[59] is chosen in this work because it ensures localness in composition space. In fact, it is capable of reproducing differential diffusion for the reduced variables using a constant C_ϕ, whose value was validated in the DNS analysis of Ref. 94.

In order to improve computational efficiency by avoiding too many notional particles gathering in one CFD cell, a particle number control is used, based on particle cloning and clustering.[55] The initial number of particles per CFD cell is $N_p = 120$, which will be shown to be sufficient for the Sandia flame series (see Sec. V A). To control the number of notional particles, a minimum of $N_{p,\min} = 0.8 \cdot N_p = 96$ and a maximum of $N_{p,\max} = 1.2 \cdot N_p = 144$ are allowed in each cell.

© Author(s) 2021

TABLE I. Parameters and their values for each model used in the TPDF method.

Parameter	Value	Applied model
C_0	2.1	Simplified Langevin model Eq. (5b)[56]
C_Ω	0.689 2	Turbulent frequency model in Eqs. (5c), (6), and (7c)[54]
$C_{\omega 1}$	0.71	
$C_{\omega 2}$	0.90	
C_3	1.0	
C_4	1.25	
C_ϕ	1.5	EMST-mixing model[59]

The boundary conditions for the mean velocities, the Reynolds stresses, the turbulent frequency, and the turbulent kinetic energy are the same as the numerical setup of Ref. 95.

For the reduced chemistry REDIM-grad [cf. Eq. (14)], the reduced coordinate vector is set to be

$$\Theta = (\theta_1, \theta_2)^{\mathrm{T}} = (\phi_{\mathrm{N_2}}, \phi_{\mathrm{CO_2}} + 0.5\phi_{\mathrm{H_2O}})^{\mathrm{T}}. \tag{28}$$

This has been seen to be a reasonable choice to couple the manifold-based reduced chemistry with the mixing process in PDF simulations. More details can be found in Ref. 86.

A. Sensitivity with respect to the particle number

In this section, the minimum number of notional particles N_p per CFD cell required for the simulation of the Sandia flame series is first investigated. Increasing values of N_p are tested, until the results reach statistical convergence. Figure 6 shows representative results for the conditional Favre-averaged H_2 mass fraction $\widetilde{w_{\mathrm{H_2}}|\xi}$ over the mixture fraction $\widetilde{\xi}$ at position $x/D_j = 7.5$, for both flames D and F using different numbers of N_p.

From Fig. 6, it is clear that for flame D, $N_p = 20$ and $N_p = 40$ do not give enough resolution, and at least a value of $N_p = 60$ is required to gain in accuracy. For flame F instead, which has a high degree of local extinction,[48] $N_p = 100$ is the minimum number of notional particles required per CFD cell. It is believed that since the flame F has a stronger turbulence and consequently higher scalar gradients in flow field, an accurate determination of the gradients [cf. Eq. (24)] for flame F requires the use of a large number of particles N_p. As a consequence, the number of notional particles $N_p = 120$ is applied for flame D–F in the next simulations.

B. Predicted velocity field

The mean $\widetilde{u}_1$ and the Reynolds stresses $\widetilde{u_1'' u_1''}$ of the axial velocity are shown in Figs. 7 and 8, where the symbols represent the experimental data.[96]

One can see that the mean axial velocities (Fig. 7) are in good agreement with the experiment, although a certain deviation is observed for flame F.

The quantities $\widetilde{u_1'' u_1''}$ (Fig. 8) are under-predicted for all three flames, but this was already observed in the literature when using RANS, such as in Refs. 97 and 98. A better prediction could be obtained by large eddy simulations (LES), as reported in e.g., Refs. 99 and 100.

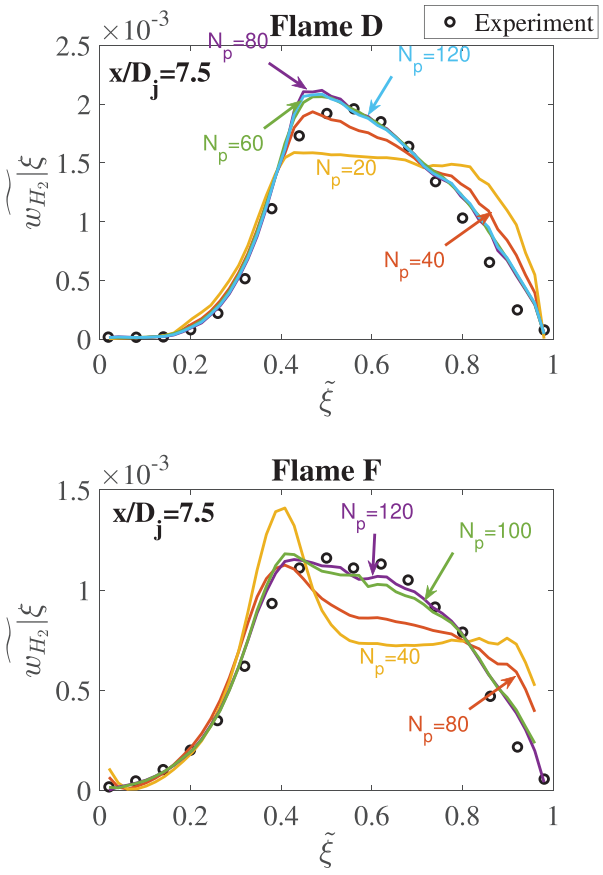

FIG. 6. Sensitivity of particle number N_p per cell for conditional Favre-averaged $\widetilde{w_{\mathrm{H_2}}}$ at position $x/D_j = 7.5$ for Sandia flames D and F. Symbols: experimental measurement.[48]

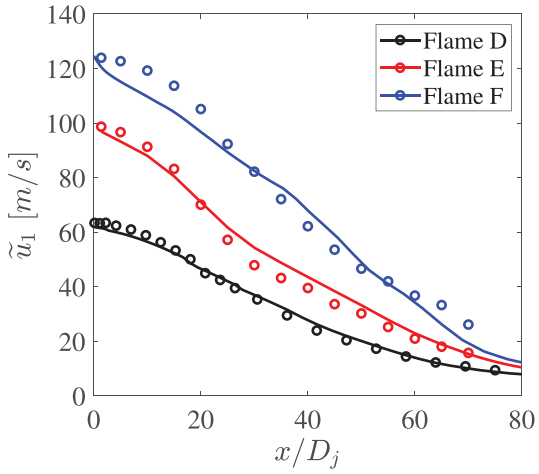

FIG. 7. Mean of axial velocity $\widetilde{u}_1$ along the centerline for Sandia D–F using four-dimensional REDIM-grad model with $N_p = 120$ notional particles. Symbols: experimental measurements;[96] lines: simulation results.

© Author(s) 2021

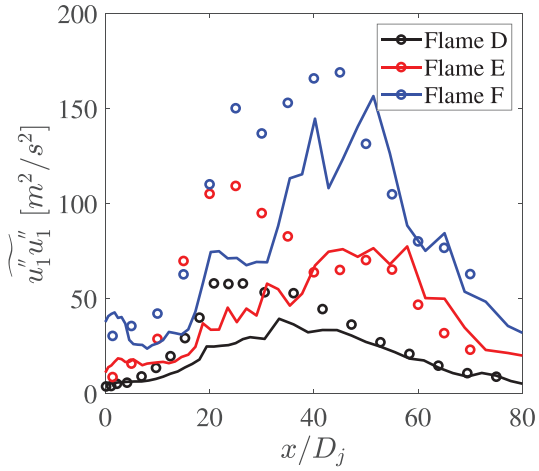

FIG. 8. Reynolds stress of axial velocity $\widetilde{u_1''u_1''}$ along the centerline for Sandia D–F using four-dimensional REDIM-grad model with $N_p = 120$ notional particles. Symbols: experimental measurements;[96] lines: simulation results.

C. Predicted thermo-kinetic quantities

In order to relate the thermo-kinetic quantities to the differential molecular diffusion effect described in Sec. V B, two additional REDIM tables are generated for the numerical simulations. The number of notional particles used in the CFD remains $N_p = 120$. The results obtained will be compared with the previously discussed REDIM-grad. The additional REDIMs are

- REDIM-ED: here the gradient estimate for the REDIM evolution equation is provided as *a priori* information. The gradients $\hat{\chi}(\theta_1)$ and $\hat{\chi}(\theta_2)$ in Eq. (12) are obtained from detailed solutions of steady flame scenarios using the equal-diffusivity (ED) transport model (Le = 1). The flame scenarios here are the steady counterflow diffusion flames with different strain rates and the pure mixing line, same as used in Ref. 84. In this case, the REDIM model is two-dimensional and parametrized as $\Psi = (\theta_1, \theta_2)$.
- REDIM-DD: This model is similar to REDIM-ED, with the only difference that the gradients $\hat{\chi}(\theta_1)$ and $\hat{\chi}(\theta_2)$ in Eq. (12) are obtained from detailed solutions of steady flame scenarios using the differential molecular diffusion (DD) transport model.

Note that the REDIM models using a gradient estimate from detailed solutions of steady flames, such as REDIM-ED and REDIM-DD, are coincident with flamelet-based models such as the flamelet generated manifold (FGM). Moreover, it should be emphasized that for the implementation of REDIM-ED and REDIM-DD one does not need to calculate the gradients of the reduced coordinates $[\mathrm{grad}(\theta_1), \mathrm{grad}(\theta_2)]$, while this step is necessary for REDIM-grad as shown in Sec. III.

1. Species CO and OH

The conditional Favre-averaged mass fractions of CO and OH over mixture fraction $\tilde{\xi}$ at three different locations ($x/D_j = 7.5$, 15, and 30) are shown in Figs. 9 and 10 for flames D–F.

It is observed that the molecular transport has minor effects on CO and moderate on OH. Therefore, for the predicted w_{CO} and w_{OH}, the results using REDIM-ED and REDIM-DD are comparable and show good agreement for flames D and E. For flame F instead, both REDIM-ED and REDIM-DD over-predict the quantities largely, indicating an under-prediction of local extinction. Overall, the REDIM-grad shows a much better prediction for flame F at most positions. For example, at position $x/D_j = 7.5$, the maximum difference between experimental measurements[48] and the REDIM-grad result is around 10%, which is much lower than the maximum difference between experimental measurements[48] and the REDIM-DD result with around 30%. The only noticeable deviation occurs at positions $x/D_j = 15$ and 30 for the conditional w_{CO} with around 15% difference related to experimental measurements.[48] However, such over-prediction was also observed in Ref. 95 (p. 100 of the supplementary material), where the ISAT chemistry model[101] was used for the detailed chemistry calculation, and the REDIM-DD model over-predicts significantly with a maximum difference of around 60% compared to experimental measurements.[48]

The reason behind a more accurate prediction of flame F using REDIM-grad is that the influence of the scalar gradients on the thermo-kinetic states has been considered. In fact, scalar gradients can account for states departing from the steady flame regime, as it will be discussed in Sec. V C 2.

2. Species H_2

In reacting flows, the effect of differential molecular diffusion on H_2 is shown to be important.[24,102,103] Figure 11 shows the conditional Favre-averaged mass fractions of H_2 over mixture fraction $\tilde{\xi}$ at three different locations ($x/D_j = 7.5$, 15, and 30) for Sandia flames D–F.

At $x/D_j = 30$, the results using REDIM-ED show already a good agreement for flame D and E, indicating that far downstream the differential molecular diffusion becomes less important and the turbulent transport more important. However, the results for REDIM-ED over-predict the quantity significantly for flame F (the difference to experimental measurements[48] can be up to 75%) because not sufficient local extinction can be captured. At $x/D_j = 7.5$ and 15, REDIM-ED largely over-predicts w_{H_2} especially within $0.4 < \xi < 0.6$ (the difference to experimental measurements[48] can be up to 50%), because in this regime the molecular diffusivity is enhanced due to high temperature. The resulting effect of differential molecular diffusion is still dominant in this range.

On the contrary, the application of REDIM-DD overestimates differential molecular diffusion (the difference to experimental measurements[48] up to 60% especially at position $x/D_j = 30$), since the influence of turbulence on reduced chemistry is not accounted for. As a consequence, both REDIM-ED and REDIM-DD do not seem suitable to correctly predict the species with high molecular diffusivity (e.g., H_2) at the positions where both molecular and turbulent diffusivity are important (e.g., here $x/D_j = 7.5$ and 15).

Although for flame F the quantity is over-predicted at $x/D_j = 30$, the results using REDIM-grad show the best agreement with experimental measurements[48] at all three positions, and the corresponding differences between the experimental measurements[48] and the REDIM-grad results are mostly less than 10%, which are obviously less than those between the experimental measurements[48] and the REDIM-ED results (up to 75%) or the REDIM-DD results (up to 60%).

Such a good agreement between numerical results and experimental measurements[48] for Sandia flame D–F indicates the that the effect of differential molecular diffusion and turbulent transport on

© Author(s) 2021

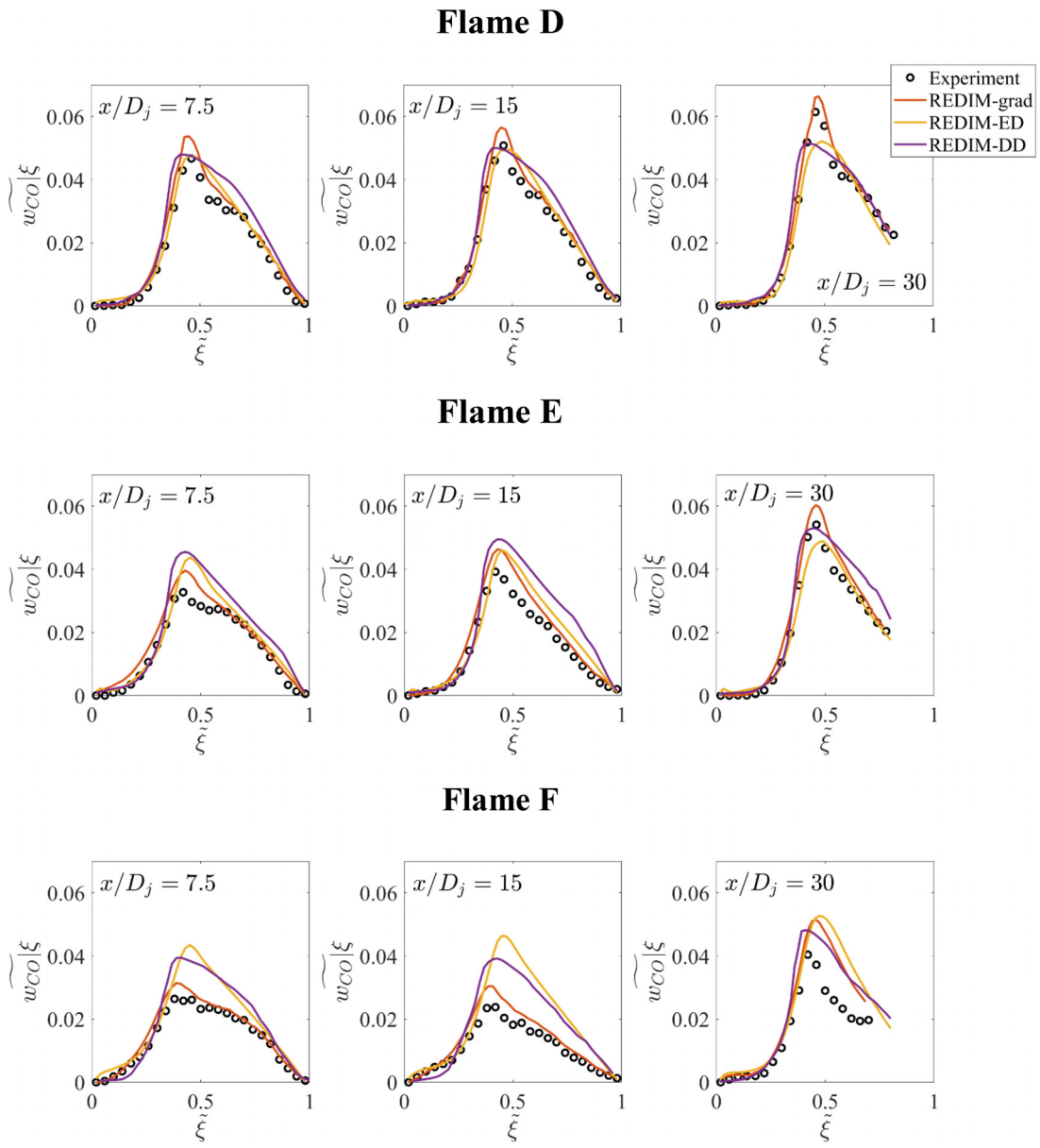

FIG. 9. Conditional Favre-averaged w_{CO} over mixture fraction at three different locations for Sandia flames D–F. Symbols: experimental measurements;[48] Red lines: REDIM-grad model; yellow lines: REDIM-ED model; purple lines: REDIM-DD model.

reduced chemistry can be indeed accounted for automatically by the REDIM method in terms of $\hat{\chi}(\Theta)$. Unlike the method proposed in Ref. 36 or in Ref. 35 where the effect of differential diffusion is considered based on two reduced chemistry groups (one group using the unity-Lewis number assumption and the other using a detailed transport model), the REDIM-grad model is generated by using the detailed transport model and captures the differential diffusion effect automatically in terms of local scalar gradients that are related to turbulence intensity.

D. Scatter plots

The results shown in Figs. 9–11 suggest that the accurate prediction of thermo-kinetic quantities must capture both the effect of turbulence on differential molecular diffusion and the degree of local extinction and re-ignition.

Flame D is selected as a representative example to discuss the effect of turbulence on differential molecular diffusion because it has a low degree of local extinction and re-ignition,[48] and both significant and non-significant effects of differential molecular diffusion can be

© Author(s) 2021

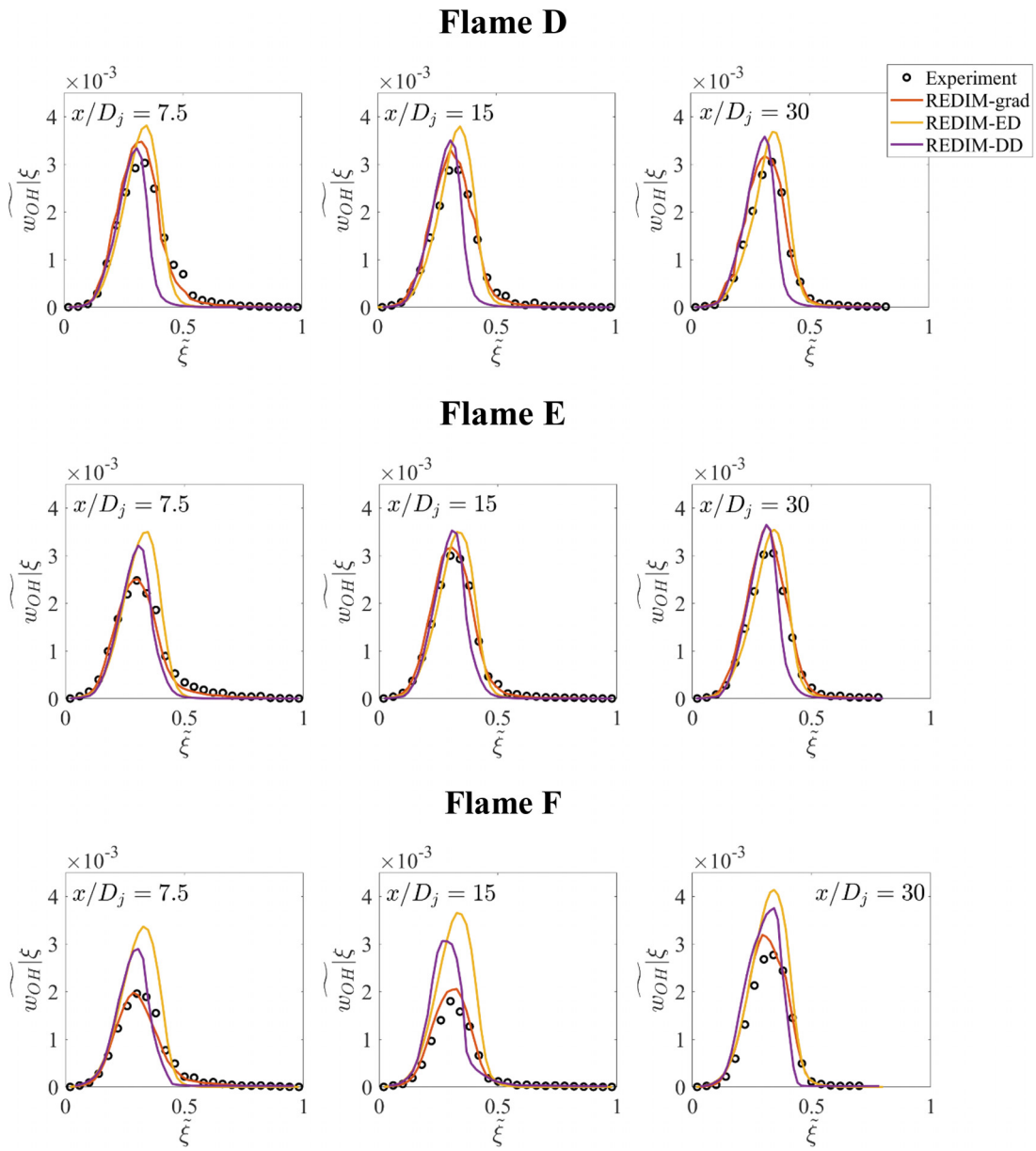

FIG. 10. Conditional Favre-averaged w_{OH} over mixture fraction at three different locations for Sandia flame D–F. Symbols: experimental measurements;[48] red lines: REDIM-grad model; yellow lines: REDIM-ED model; purple lines: REDIM-DD model.

observed depending on spatial positions. As shown in Fig. 11, both REDIM-ED and REDIM-DD models cannot predict well the H_2 mass fractions at $x/D_j = 7.5$ and 15 (high degree of differential diffusion, cf. Fig. 17), while the REDIM-ED model is suitable for the prediction at position $x/D_j = 30$. Therefore, it is interesting to see how the thermo-kinetic states are distributed compared with REDIM-ED and REDIM-DD, which are shown in Figs. 12 and 13. The blue mesh represents the REDIM-ED, the red mesh the REDIM-DD. It can be seen that at $x/D_j = 7.5$ most scatter points (around 75% of the scatter points) are located between REDIM-ED and REDIM-DD, explaining why REDIM-ED over-predicts and REDIM-DD under-predicts the mass fractions of H_2 at this position (cf. Fig. 11). At $x/D_j = 30$, most scatter points are closer to or above the REDIM-ED surface. More precisely, approximately 30% scatter points located between REDIM-ED and REDIM-DD surfaces are closer to the REDIM-ED surface, while approximately 60% scatter points are above the REDIM-ED surface. This indicates that the REDIM-ED is indeed sufficient for the prediction of the thermo-kinetic quantities in this section.

Besides the effect of turbulence on differential molecular diffusion, an accurate estimation of local extinction and re-ignition

© Author(s) 2021

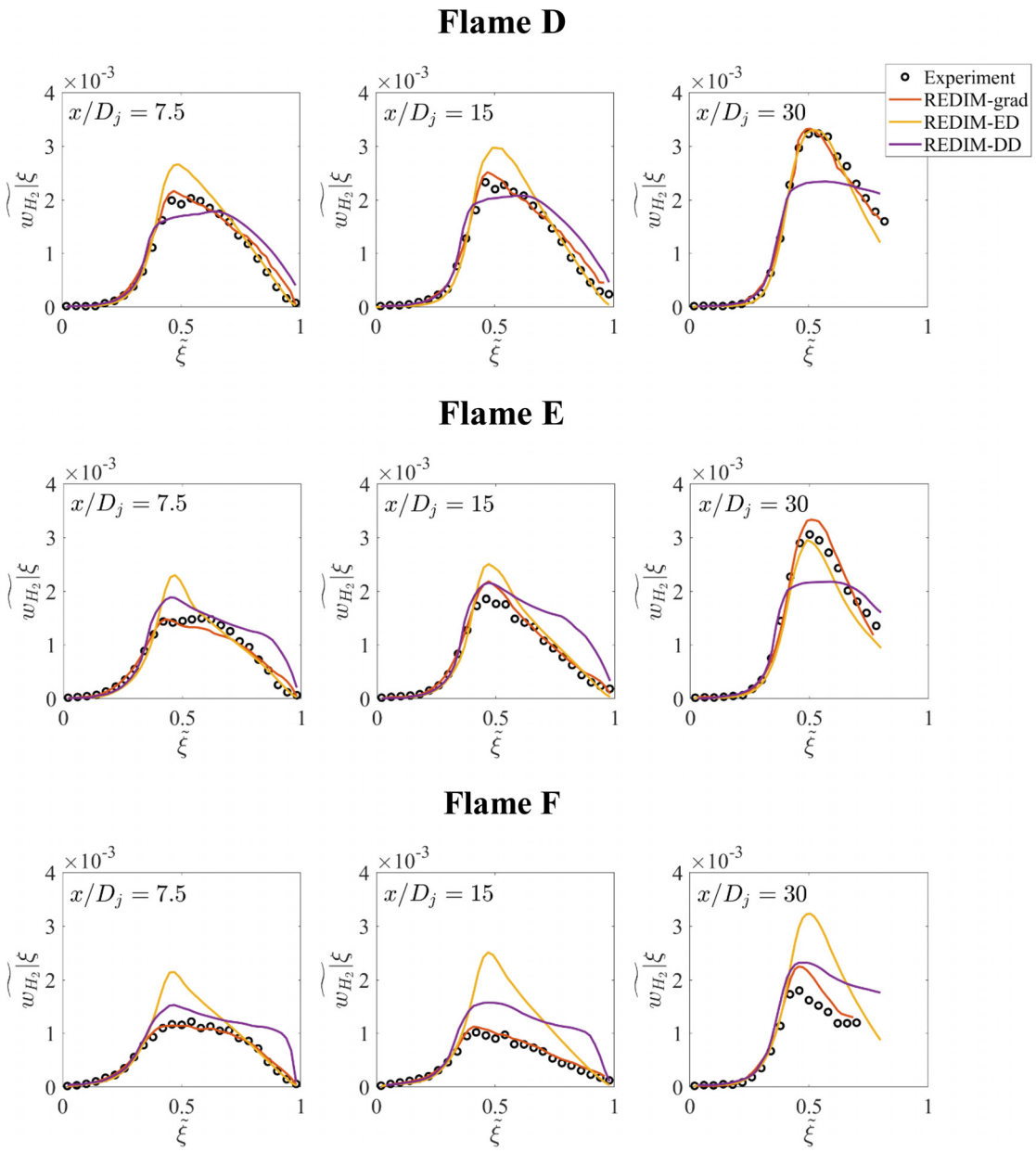

FIG. 11. Conditional Favre-averaged w_{H_2} over mixture fraction at three different locations for Sandia flame D–F. Symbols: experimental measurements;[48] red lines: REDIM-grad model; Yellow lines: REDIM-ED model; Purple lines: REDIM-DD model.

is important for flames E and F, featuring moderate and high turbulence levels. Figure 14 shows the scatter data of w_{H_2} vs the mixture fraction for the experiment[48] and the REDIM-grad simulation at three different positions ($x/D_j = 7.5$, 15, and 30) for flame F (same conclusions apply to flame E). The results are consistent with the conditional Favre-averaged results shown in Fig. 11 for flame F. At both positions $x/D_j = 7.5$ and 15, the high degree of local extinction can be well predicted by using the proposed algorithm (REDIM-grad). At $x/D_j = 30$, the simulation gives less local extinction compared to the experimental measurement,[48] or alternatively, a stronger re-ignition is observed. This is consistent with the results shown in Fig. 11: the conditional w_{H_2} at position $x/D_j = 30$ predicted by REDIM-grad is higher than the experimental value.[48]

E. Validation of one-directional gradient approximation

We have shown so far that the REDIM-grad is suitable to capture the effect of differential diffusion on thermo-kinetic states in turbulent

© Author(s) 2021

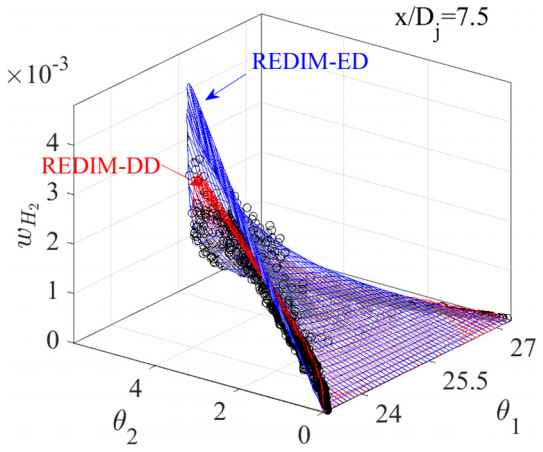

FIG. 12. Scatter plots of mass fraction of H_2 over θ_1 and θ_2 at position $x/D_j = 7.5$ for flame D. Scatter plots: predicted by four-dimensional REDIM-grad model; blue mesh: system states predicted by REDIM-ED; red mesh: system states predicted by REDIM-DD.

flows. It is also interesting to see whether the direction of $\nabla\Theta$ and $\mathbf{n}_\xi$ overlaps or not. If both directions almost overlap ($\angle(\mathbf{n}_\xi, \nabla\Theta) \approx 0^\circ$ or 180°), it can be concluded that we can indeed consider the system locally as one-dimensional and the directional derivative $\nabla_{\mathbf{n}_\xi}\Theta$ represents the main gradient, which has the major contribution on the chemistry.

Figure 15 shows the probability density (PDF) of the angle between $\mathbf{n}_\xi$ and $\nabla\theta_2$, $\alpha = \angle(\mathbf{n}_\xi, \nabla\theta_2)$ at three different positions for Sandia flame D–F. It is observed that in all cases the angles are mostly either 0° or 180°. The same also applies for $\angle(\mathbf{n}_\xi, \nabla\theta_1)$, which is not shown here. It is therefore observed that the direction of the gradients of the chosen reduced coordinates $\Theta = (\theta_1, \theta_2)^{\mathrm{T}} = (\phi_{\mathrm{N_2}}, \phi_{\mathrm{CO_2}} + 0.5\phi_{\mathrm{H_2O}})^{\mathrm{T}}$ is coincident with the direction of $\mathbf{n}_\xi$, and there is no need to consider the tangential gradient along the iso-ξ-line.

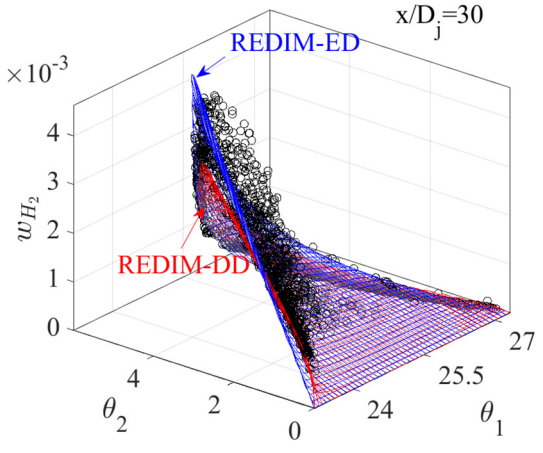

FIG. 13. Scatter plots of mass fraction of H_2 over θ_1 and θ_2 at position $x/D_j = 30$ for flame D. Scatter plots: predicted by four-dimensional REDIM-grad model; blue mesh: system states predicted by REDIM-ED;red mesh: system states predicted by REDIM-DD.

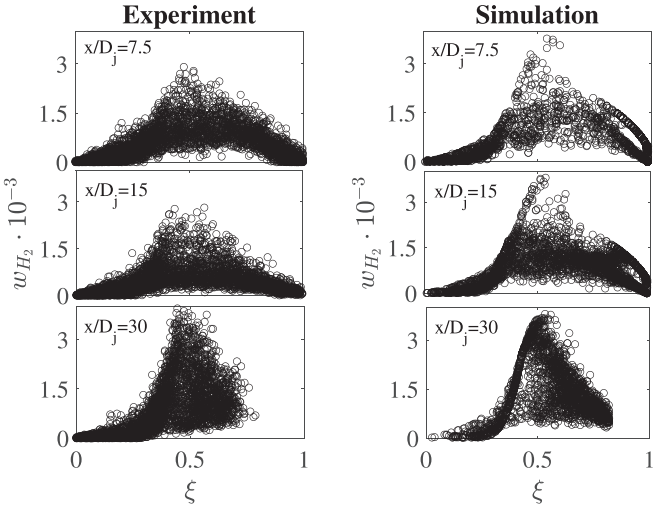

FIG. 14. Scatter plots of mass fraction of H_2 over mixture fraction at three different positions for flame F. Left: experimental data;[48] Right: simulation results using REDIM-grad.

For species H_2 on the other hand, tangential diffusion (corresponding to the tangential gradient along the *iso*-ξ-surface) was seen to be important in turbulent flows due to the high molecular diffusivity of H_2,[23,24] as it strongly influences the chemistry.[24] It is worth to investigate the direction of the gradient of H_2. Figure 16 shows the probability density (PDF) of the angle between $\mathbf{n}_\xi$ and ∇H_2, $\alpha = \angle(\mathbf{n}_\xi, \nabla H_2)$, at three different positions for Sandia flame D (the same conclusion applies to Sandia flame E and F). At position $x/D_j = 30$ where the degree of differential diffusion is low, we notice that $\alpha = \angle(\mathbf{n}_\xi, \nabla H_2) \approx 0^\circ$. However at positions $x/D_j = 7.5$ and 15 where one has moderate to high degrees of differential molecular diffusion (cf. Fig. 17) the pdf values for $\alpha = \angle(\mathbf{n}_\xi, \nabla H_2)$ are mostly in the range of $0^\circ - 60^\circ$ and $120^\circ - 180^\circ$. This means that for H_2 a tangential gradient along the iso-ξ-line exists almost everywhere. Therefore, the use of H_2 in the reduced coordinates does not seem suitable for the *one-directional gradient approximation* used in this work because the effect of the tangential gradient on the reduced chemistry has not been accounted for. In other words, if the species with high molecular diffusivity (e.g., H_2) are considered as reduced coordinates (e.g., $\theta = \phi_{\mathrm{CO_2}} + \phi_{\mathrm{H_2O}} + \phi_{\mathrm{H_2}}$[104]) the effect of the tangential gradient must be as well considered in the calculation. Under such circumstances, the algorithm proposed in Ref. 46 should be used for the REDIM generation instead.

F. Analysis of the degree of differential diffusion

To assess the effect of turbulence on molecular transport for the Sandia flame series, the degree of differential molecular diffusion γ_{DD}, introduced in Refs. 30 and 35, can be useful. In Ref. 35, a ratio between molecular diffusivity (physical transport property, $\mathscr{D}_m$) and turbulent diffusivity (modeled transport property, $\mathscr{D}_t$) is introduced to represent the degree of differential molecular diffusion

© Author(s) 2021

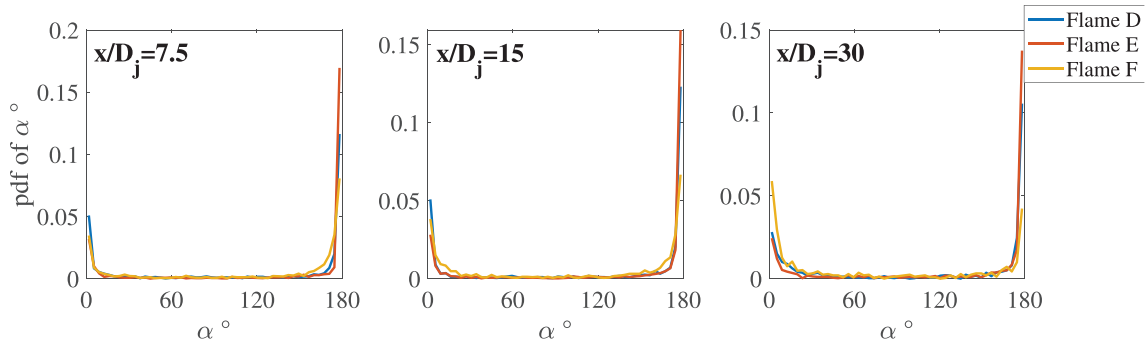

FIG. 15. Probability density of angle between $\mathbf{n}_\xi$ and $\nabla\theta_2$, $\alpha = \angle(\mathbf{n}_\xi, \nabla\theta_2)$ at three different positions for Sandia flame D–F.

$$\gamma_{\mathrm{DD}} = \frac{\mathscr{D}_m}{\mathscr{D}_m + \mathscr{D}_t}. \tag{29}$$

γ_{DD} vanishes ($\gamma_{\mathrm{DD}} \to 0$) if $\mathscr{D}_t \gg \mathscr{D}_m$, meaning that the flow has a low degree of differential molecular diffusion, and it is dominated by turbulent transport. On the other hand, $\gamma_{\mathrm{DD}} \to 1$ for $\mathscr{D}_m \gg \mathscr{D}_t$ means that the flow has a high degree of differential molecular diffusion.

In the framework of the RANS method, the turbulent diffusivity can be modeled as:[30] $\mathscr{D}_t = (C_\mu/Sc_t) \cdot (k^2/\epsilon)$, where the model constant is $C_\mu = 0.09$. Sc_t is the turbulent Schmidt number, k is the turbulent kinetic energy, and ϵ is the turbulent dissipation. The turbulent diffusivity $\mathscr{D}_t$ is related to the turbulence Reynolds number Re_L where the characteristic length scale is defined as $L = k^{3/2}/\varepsilon$:[30,56,78] $Re_L = (k^{1/2} \cdot L)/\nu$, where ν is the kinematic viscosity. Thus, Eq. (29) can be reformulated as

$$\gamma_{\mathrm{DD}} = \frac{\mathscr{D}_m}{\mathscr{D}_m + \dfrac{C_\mu}{Sc_t} \cdot \nu \cdot Re_L}. \tag{30}$$

It is evident that by increasing Reynolds number, the degree of differential molecular diffusion γ_{DD} decreases monotonically and the turbulent transport plays a dominant role. In the calculation of γ_{DD} [see Eq. (30)] for Sandia flame series, we follow the setup in Ref. 30: the turbulent Schmidt number Sc_t is set to 0.85; The molecular diffusivity and viscosity are approximated, respectively, as $\nu = 1.57 \times 10^{-5}(\mathrm{T}/294\,\mathrm{K})^{1.70}$ and $\mathscr{D}_m = 2.06 \times 10^{-5}(\mathrm{T}/294\,\mathrm{K})^{1.70}$.

Figure 17 shows radial profiles of γ_{DD} at three different axial positions ($x/D_j = 7.5$, 15, and 30) for all three flame configurations. Two important observations should be addressed here, which have also been confirmed in, e.g., Ref. 30:

- γ_{DD} reaches its maximum at $r/D_j \approx 1.0$. This is the position of the temperature peak, associated with a high the molecular diffusivity $\mathscr{D}_m$.[30]
- The effect of molecular diffusion becomes less significant (decreasing γ_{DD}) moving further downstream, consistent with the results in Fig. 11 showing that at position $x/D_j = 30$ the REDIM-ED (unity-Lewis number assumption) is good enough for the prediction of H_2 concentrations, while upstream ($x/D_j = 7.5$ and 15) the instantaneous scalar gradients on REDIM reduced chemistry (REDIM-grad) are needed.

To summarize, the effect of differential molecular diffusion can be well captured by the REDIM model taking into account the effect of scalar gradients on the chemistry automatically, and no additional models for the transport properties such as unity-Lewis number assumption are necessary.

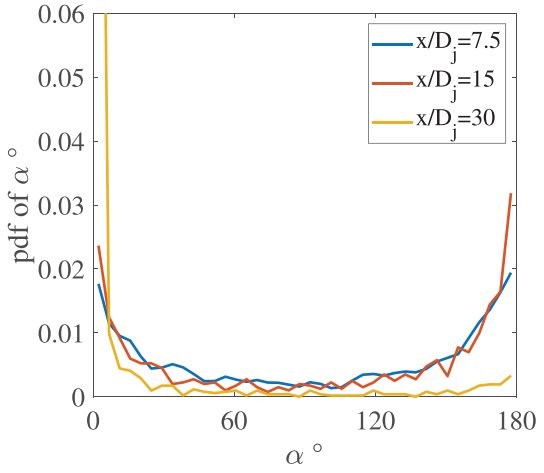

FIG. 16. Probability density of angle between $\mathbf{n}_\xi$ and ∇H_2, $\alpha = \angle(\mathbf{n}_\xi, \nabla H_2)$ at three different positions for Sandia flame D.

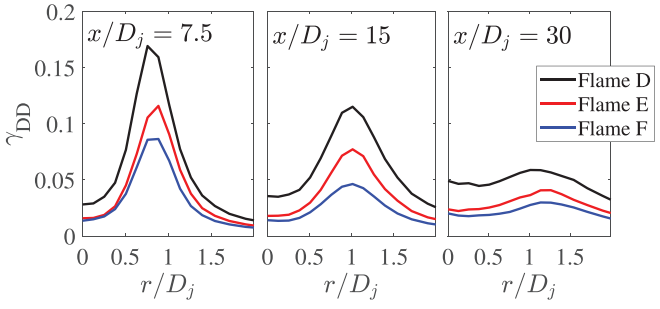

FIG. 17. Radial profiles of degree of differential molecular diffusion γ_{DD} at three different axial positions ($x/D_j = 7.5$, 15, and 30) for Sandia flame series.

© Author(s) 2021

G. Computational time

Although the results based on REDIM-grad and the *one-directional gradient approximation* show a very good agreement with the experimental data, it is worth to discuss the computational time required by this computation. For the evolution of the thermo-kinetic states due to reaction, the source terms of the reduced variables are *pre-tabulated*. For the reduced chemistry expressed as $\mathscr{M} = \{\Psi : \Psi = \Psi(\Theta)\}$ (e.g., REDIM-ED and REDIM-DD in this work), the source terms are stored as $\mathbf{F}(\Theta)$. However, for the reduced chemistry in form of $\mathscr{M} = \{\Psi : \Psi = \Psi(\Theta, \chi(\Theta))\}$ (e.g., REDIM-grad in this work), the source terms are stored as $\mathbf{F}(\Theta, \chi(\Theta))$. Compared to the REDIM-ED and REDIM-DD models, the application of REDIM-grad requires the determination of gradients $\chi(\Theta^*)$ for each notional particle as an additional step. Furthermore, the interpolation routine for the table lookup to retrieve the source terms requires higher central processing unit (CPU) times for REDIM-grad than for REDIM-ED and REDIM-DD. In this work, a series of loops is used to determine the gradients of each particle, so that the calculation using the four-dimensional REDIM-grad is about 4 times slower than using the two-dimensional REDIM-ED and two-dimensional REDIM-DD. More precisely, for the simulation using $N_p = 120$ notional particles per cell and totally 2142 CFD cells in the present work, the overall computational time for the whole simulation with 36 CPU cores using the two-dimensional REDIM-ED or the two-dimensional REDIM-DD is around 10 h (0.4 days) in average, while using the four-dimensional REDIM-grad it is around 45 h (1.9 days). A certain speed-up is expected if moving to parallel loops. However, the CPU time required by REDIM-grad is still expected to be larger than REDIM-ED and REDIM-DD. To summarize, in the framework of the REDIM method much more accurate predictions of the thermo-chemical quantities could be obtained using the REDIM-grad in this work, at the cost of an increased computational time.

VI. CONCLUSIONS

This work focuses on the use of REDIM reduced chemistry for numerical simulations of turbulent non-premixed flames. A novel method has been proposed to consider the differential diffusion in the REDIM model for the turbulent reactive simulations. The REDIM model has been parametrized by selected reduced variables Θ and their gradients grad(Θ). Since the transport coefficients are physical properties that are not affected by the external flow, a detailed transport model is considered to build the transport matrix. The effect of turbulence on differential molecular diffusion is considered through the gradients of the reduced variables grad(Θ). The *one-directional gradient approximation* is proposed in this work to locally treat the flame as one-dimensional, so that the REDIM reduced chemistry generated using one-dimensional directional gradients can also represent the system with multi-directional gradients (REDIM-grad model). Furthermore, it is assumed that the sub-grid gradients can be approximated by the gradients calculated through the PDF particle field. The well-known turbulent non-premixed jet flames, Sandia D–F, are selected for validation. The results show that the REDIM-grad can capture the effect of turbulence on differential molecular diffusion and the degree of local extinction very well, so that the simulation can reproduce the experimental measurement with good accuracy. However, such accuracy has the drawback of having a higher computational cost. Further investigations aimed to find a possible correlation between scalar gradients are required, in order to reduce the dimensions of the proposed model (REDIM-grad). The approximation of the real sub-grid gradients being represented by the gradients of the particle fields is a model assumption, which in principle needs further investigation. Room of improvement is also given by the calculation of the reduced variable gradients at run-time, which can be further optimized to reduce the computational cost.

ACKNOWLEDGMENTS

We gratefully acknowledge financial support from the German Research Foundation (DFG) within the DFG/MOST project MA 1205/26 (C. Yu and U. Maas), the ONR-USA Project No. 2.20.1907 (288) (F. Minuzzi) and the DFG in the framework of the Sonder-Forschungsbereich Transregio 40 (P. Breda and M. Pfitzner). Additionally, the authors are thankful to Professor Andreas Class (Institut fuer Kern-und Energietechnik, KIT) for many helpful discussions.

The authors confirm that ethical standards have been obeyed.

The authors declare that they have no conflict of interest.

DATA AVAILABILITY

The data that support the findings of this study are available from the corresponding author upon reasonable request.

REFERENCES

[1]D. A. Goussis and U. Maas, "Model reduction for combustion chemistry," in *Turbulent Combustion Modeling* (Springer, 2011), pp. 193–220.
[2]U. Maas and A. S. Tomlin, "Time-scale splitting-based mechanism reduction," in *Cleaner Combustion* (Springer, 2013), pp. 467–484.
[3]T. Turányi and A. S. Tomlin, *Analysis of Kinetic Reaction Mechanisms* (Springer, 2014).
[4]U. Maas and D. Thévenin, "Correlation analysis of direct numerical simulation data of turbulent non-premixed flames," in *Symposium (International) on Combustion* (Elsevier, 1998), Vol. 27, pp. 1183–1189.
[5]U. Maas and S. B. Pope, "Simplifying chemical kinetics: Intrinsic low-dimensional manifolds in composition space," Combust. Flame **88**, 239–264 (1992).
[6]O. Gicquel, N. Darabiha, and D. Thévenin, "Laminar premixed hydrogen/air counterflow flame simulations using flame prolongation of ILDM with differential diffusion," Proc. Combust. Inst. **28**, 1901–1908 (2000).
[7]N. Peters, "Laminar diffusion flamelet models in non-premixed turbulent combustion," Prog. Energy Combust. Sci. **10**, 319–339 (1984).
[8]J. Van Oijen and L. De Goey, "Modelling of premixed counterflow flames using the flamelet-generated manifold method," Combust. Theory Modell. **6**, 463–478 (2002).
[9]V. Bykov and U. Maas, "The extension of the ILDM concept to reaction-diffusion manifolds," Combust. Theory Modell. **11**, 839–862 (2007).
[10]A. Aspden, M. Day, and J. B. Bell, "Three-dimensional direct numerical simulation of turbulent lean premixed methane combustion with detailed kinetics," Combust. Flame **166**, 266–283 (2016).
[11]E. R. Hawkes, R. Sankaran, J. C. Sutherland, and J. H. Chen, "Direct numerical simulation of turbulent combustion: Fundamental insights towards predictive models," J. Phys.: Conf. Ser. **16**, 65 (2005).
[12]A. W. Cook and J. J. Riley, "Subgrid-scale modeling for turbulent reacting flows," Combust. Flame **112**, 593–606 (1998).
[13]Y. Lee and S. Pope, "Nonpremixed turbulent reacting flow near extinction," Combust. Flame **101**, 501–528 (1995).
[14]J. Doom, Y. Hou, and K. Mahesh, "A numerical method for DNS/LES of turbulent reacting flows," J. Comput. Phys. **226**, 1136–1151 (2007).
[15]J. Lai and N. Chakraborty, "Effects of Lewis number on head on quenching of turbulent premixed flames: A direct numerical simulation analysis," Flow, Turbul. Combust. **96**, 279–308 (2016).

© Author(s) 2021

[16]S. Vo, A. Kronenburg, O. T. Stein, and E. R. Hawkes, "Direct numerical simulation of non-premixed syngas combustion using OpenFOAM," in *High Performance Computing in Science and Engineering '16* (Springer, 2016), pp. 245–257.

[17]L. Smith, R. Dibble, L. Talbot, R. Barlow, and C. Carter, "Laser Raman scattering measurements of differential molecular diffusion in turbulent nonpremixed jet flames of H_2-CO_2 fuel," Combust. Flame **100**, 153–160 (1995).

[18]M. B. Long, S. H. Stirner, and R. W. Bilger, "Differential diffusion in jets using joint PLIF and Lorenz-Mie imaging," Combust. Sci. Technol. **92**, 209–224 (1993).

[19]R. Barlow, G. Fiechtner, C. Carter, and J.-Y. Chen, "Experiments on the scalar structure of turbulent CO/H_2/N_2 jet flames," Combust. Flame **120**, 549–569 (2000).

[20]R. W. Dibble and M. B. Long, "Investigation of differential diffusion in turbulent jet flows using planar laser Rayleigh scattering," Combust. Flame **143**, 644–649 (2005).

[21]S. S. Shy, M. T. Nguyen, S.-Y. Huang, and C.-C. Liu, "Is turbulent facilitated ignition through differential diffusion independent of spark gap?," Combust. Flame **185**, 1–3 (2017).

[22]S. Shy, M. T. Nguyen, and S. Y. Huang, "Effects of electrode spark gap, differential diffusion, and turbulent dissipation on two distinct phenomena: Turbulent facilitated ignition versus minimum ignition energy transition," Combust. Flame **205**, 371–377 (2019).

[23]W. Han, A. Scholtissek, and C. Hasse, "The role of tangential diffusion in evaluating the performance of flamelet models," Proc. Combust. Inst. **37**, 1767–1774 (2019).

[24]W. Han, A. Scholtissek, F. Dietzsch, and C. Hasse, "Thermal and chemical effects of differential diffusion in turbulent non-premixed H_2 flames," Proc. Combust. Inst. (published online 2020).

[25]R. Hilbert and D. Thßvenin, "Influence of differential diffusion on maximum flame temperature in turbulent nonpremixed hydrogen/air flames," Combust. Flame **138**, 175–187 (2004).

[26]J. Sutherland, P. Smith, and J. Chen, "Quantification of differential diffusion in nonpremixed systems," Combust. Theory Modell. **9**, 365–383 (2005).

[27]A. Aspden, M. Day, and J. Bell, "Lewis number effects in distributed flames," Proc. Combust. Inst. **33**, 1473–1480 (2011).

[28]D. O. Lignell, J. C. Hewson, and J. H. Chen, "*A-priori* analysis of conditional moment closure modeling of a temporal ethylene jet flame with soot formation using direct numerical simulation," Proc. Combust. Inst. **32**, 1491–1498 (2009).

[29]A. Vranos, B. Knight, W. Proscia, L. Chiappetta, and M. Smooke, "Nitric oxide formation and differential diffusion in a turbulent methane-hydrogen diffusion flame," in *Symposium (International) on Combustion* (Elsevier, 1992), Vol. 24, pp. 377–384.

[30]H. Wang and K. Kim, "Effect of molecular transport on pdf modeling of turbulent non-premixed flames," Proc. Combust. Inst. **35**, 1137–1145 (2015).

[31]L. Dialameh, M. Cleary, and A. Klimenko, "A multiple mapping conditioning model for differential diffusion," Phys. Fluids **26**, 025107 (2014).

[32]J.-Y. Chen and W.-C. Chang, "Modeling differential diffusion effects in turbulent nonreacting/reacting jets with stochastic mixing models," Combust. Sci. Technol. **133**, 343–375 (1998).

[33]H. Zhou, T. Yang, and Z. Ren, "Differential diffusion modeling in LES/FDF simulations of turbulent flames," AIAA J. **57**, 3206–3212 (2019).

[34]H. Pitsch and N. Peters, "A consistent flamelet formulation for non-premixed combustion considering differential diffusion effects," Combust. Flame **114**, 26–40 (1998).

[35]H. Wang, "Consistent flamelet modeling of differential molecular diffusion for turbulent non-premixed flames," Phys. Fluids **28**, 035102 (2016).

[36]H. Pitsch, "Unsteady flamelet modeling of differential diffusion in turbulent jet diffusion flames," Combust. Flame **123**, 358–374 (2000).

[37]P. Breda, C. Yu, U. Maas, and M. Pfitzner, "Validation of an Eulerian stochastic fields solver coupled with reaction-diffusion manifolds on LES of methane/air non-premixed flames," Flow Turbulent Combust. (published online).

[38]J. O. Hirschfelder, C. F. Curtiss, R. B. Bird, and M. G. Mayer, *Molecular Theory of Gases and Liquids* (Wiley, New York, 1964), Vol. 165.

[39]E. S. Richardson and J. H. Chen, "Application of pdf mixing models to premixed flames with differential diffusion," Combust. Flame **159**, 2398–2414 (2012).

[40]A. Kronenburg and R. Bilger, "Modelling of differential diffusion effects in nonpremixed nonreacting turbulent flow," Phys. Fluids **9**, 1435–1447 (1997).

[41]S. Viswanathan, H. Wang, and S. B. Pope, "Numerical implementation of mixing and molecular transport in LES/PDF studies of turbulent reacting flows," J. Comput. Phys. **230**, 6916–6957 (2011).

[42]A. Fiolitakis, P. Ess, P. Gerlinger, and M. Aigner, "Transported PDF calculations of a turbulent, non-premixed, non-piloted, hydrogen-air flame with differential diffusion," AIAA Paper No. 2012-0179, 2012.

[43]G. Steinhilber and U. Maas, "Reaction-diffusion manifolds for unconfined, lean premixed, piloted, turbulent methane/air systems," Proc. Combust. Inst. **34**, 217–224 (2013).

[44]A. Neagos, V. Bykov, and U. Maas, "Study of extinction limits of diluted hydrogen-air counter-flow diffusion flames with the REDIM method," Combust. Sci. Technol. **186**, 1502–1516 (2014).

[45]C. Yu, F. Minuzzi, and U. Maas, "REDIM reduced chemistry for the simulation of counterflow diffusion flames with oscillating strain rates," Combust. Theory Modell. **24**, 682–704 (2020).

[46]R. Schießl, V. Bykov, U. Maas, A. Abdelsamie, and D. Thévenin, "Implementing multi-directional molecular diffusion terms into reaction diffusion manifolds (REDIMs)," Proc. Combust. Inst. **36**, 673–679 (2017).

[47]N. Peters, *Turbulent Combustion* (Cambridge University Press, 2000).

[48]R. Barlow and J. Frank, "Effects of turbulence on species mass fractions in methane/air jet flames," in *Symposium (International) on Combustion* (Elsevier, 1998), Vol. 27, pp. 1087–1095.

[49]E. O'Brien, "The probability density function (pdf) approach to reacting turbulent flows," in *Turbulent Reacting Flows* (Springer, 1980), pp. 185–218.

[50]E. O'Brien, "Statistical methods in reacting turbulent flows," AIAA J. **19**, 366–371 (1981).

[51]C. Dopazo and E. E. O'Brien, "Functional formulation of nonisothermal turbulent reactive flows," Phys. Fluids **17**, 1968–1975 (1974).

[52]S. B. Pope, "PDF methods for turbulent reactive flows," Prog. Energy Combust. Sci. **11**, 119–192 (1985).

[53]M. Muradoglu, S. B. Pope, and D. A. Caughey, "The hybrid method for the PDF equations of turbulent reactive flows: Consistency conditions and correction algorithms," J. Comput. Phys. **172**, 841–878 (2001).

[54]P. Van Slooten, Jayesh, and S. Pope, "Advances in PDF modeling for inhomogeneous turbulent flows," Phys. Fluids **10**, 246–265 (1998).

[55]D. C. Haworth, "Progress in probability density function methods for turbulent reacting flows," Prog. Energy Combust. Sci. **36**, 168–259 (2010).

[56]S. B. Pope, *Turbulent Flows* (Cambridge University Press, 2000).

[57]C. Dopazo and E. E. O'Brien, "An approach to the autoignition of a turbulent mixture," Acta Astronaut. **1**, 1239–1266 (1974).

[58]R. O. Fox, *Computational Models for Turbulent Reacting Flows* (Cambridge University Press, 2003).

[59]S. Subramaniam and S. Pope, "A mixing model for turbulent reactive flows based on Euclidean minimum spanning trees," Combust. Flame **115**, 487–514 (1998).

[60]A. Y. Klimenko and S. Pope, "The modeling of turbulent reactive flows based on multiple mapping conditioning," Phys. Fluids **15**, 1907–1925 (2003).

[61]D. Meyer and P. Jenny, "A mixing model for turbulent flows based on parameterized scalar profiles," Phys. Fluids **18**, 035105 (2006).

[62]C. Celis and L. F. F. da Silva, "Lagrangian mixing models for turbulent combustion: Review and prospects," Flow, Turbul. Combust. **94**, 643–689 (2015).

[63]P. Golda, A. Blattmann, A. Neagos, V. Bykov, and U. Maas, "Implementation problems of manifolds-based model reduction and their generic solution," Combust. Theory Modell. **24**, 377–406 (2020).

[64]U. Maas and V. Bykov, "The extension of the reaction/diffusion manifold concept to systems with detailed transport models," Proc. Combust. Inst. **33**, 1253–1259 (2011).

[65]V. Bykov, A. Neagos, A. Klimenko, and U. Maas, "Hierarchical structure of slow manifolds of reacting flows," Z. Phys. Chem. **229**, 833 (2015).

[66]W. Bilger and R. Dibble, "Differential molecular diffusion effects in turbulent mixing," Combust. Sci. Technol. **28**, 161–172 (1982).

[67]S. H. Kim and H. Pitsch, "Scalar gradient and small-scale structure in turbulent premixed combustion," Phys. Fluids **19**, 115104 (2007).

© Author(s) 2021

[68]S. Fischer, D. Markus, A. Ghorbani, and U. Maas, "PDF simulations of the ignition of hydrogen/air, ethylene/air and propane/air mixtures by hot transient jets," Z. Phys. Chem. **231**, 1773–1796 (2017).
[69]C. Strassacker, V. Bykov, and U. Maas, "REDIM reduced modeling of quenching at a cold wall including heterogeneous wall reactions," Int. J. Heat Fluid Flow **69**, 185–193 (2018).
[70]C. Strassacker, V. Bykov, and U. Maas, "REDIM reduced modeling of flame quenching at a cold wall–the influence of detailed transport models and detailed mechanisms," Combust. Sci. Technol. **191**, 208–222 (2019).
[71]A. Lipatnikov, *Fundamentals of Premixed Turbulent Combustion* (CRC Press, 2012).
[72]A. N. Lipatnikov, "Stratified turbulent flames: Recent advances in understanding the influence of mixture inhomogeneities on premixed combustion and modeling challenges," Prog. Energy Combust. Sci. **62**, 87–132 (2017).
[73]R. Bilger, "The structure of turbulent nonpremixed flames," in *Symposium (International) on Combustion* (Elsevier, 1989), Vol. 22, pp. 475–488.
[74]H. Kolla, J. Rogerson, N. Chakraborty, and N. Swaminathan, "Scalar dissipation rate modeling and its validation," Combust. Sci. Technol. **181**, 518–535 (2009).
[75]A. Karpetis and R. Barlow, "Measurements of scalar dissipation in a turbulent piloted methane/air jet flame," Proc. Combust. Inst. **29**, 1929–1936 (2002).
[76]D. Geyer, A. Kempf, A. Dreizler, and J. Janicka, "Scalar dissipation rates in isothermal and reactive turbulent opposed-jets: 1-D-Raman/Rayleigh experiments supported by LES," Proc. Combust. Inst. **30**, 681–689 (2005).
[77]C. Yu, X. Li, C. Wu, A. Neagos, and U. Maas, "Automatic construction of REDIM reduced chemistry with a detailed transport and its application to CH4 counterflow flames," Energy Fuels **34**, 16572 (2020).
[78]T. Poinsot and D. Veynante, *Theoretical and Numerical Combustion* (RT Edwards, Inc., 2005).
[79]J. Warnatz, U. Maas, R. W. Dibble, and J. Warnatz, *Combustion* (Springer, 2006).
[80]R. Cant and E. Mastorakos, *An Introduction to Turbulent Reacting Flows* (Imperial College Press, 2008).
[81]U. Maas and J. Warnatz, "Ignition processes in hydrogen oxygen mixtures," Combust. Flame **74**, 53–69 (1988).
[82]E. Eastman, "Theory of the Soret effect," J. Am. Chem. Soc. **50**, 283–291 (1928).
[83]S. Burke and T. Schumann, "Diffusion flames," Ind. Eng. Chem. **20**, 998–1004 (1928).
[84]C. Yu, F. Minuzzi, and U. Mass, "Numerical simulation of turbulent flames based on a hybrid RANS/transported-PDF method and REDIM method," Eurasian Chem.-Technol. J. **20**, 23–31 (2018).
[85]F. Minuzzi, C. Yu, and U. Maas, "Simulation of methane/air non-premixed turbulent flames based on REDIM simplified chemistry," Flow, Turbul. Combust. **103**, 963–984 (2019).
[86]C. Yu, V. Bykov, and U. Maas, "Coupling of simplified chemistry with mixing processes in PDF simulations of turbulent flames," Proc. Combust. Inst. **37**, 2183–2190 (2019).
[87]C. Yu, P. Breda, M. Pfitzner, and U. Maas, "Coupling of mixing models with manifold based simplified chemistry in PDF modeling of turbulent reacting flows," Proc. Combust. Inst. (published online 2020).
[88]S. Pope, "Consistent modeling of scalars in turbulent flows," Phys. Fluids **26**, 404–408 (1983).
[89]R. Sykes, W. Lewellen, and S. Parker, "A turbulent-transport model for concentration fluctuations and fluxes," J. Fluid Mech. **139**, 193–218 (1984).
[90]A. Zhou, J. Klewicki, and S. Pirozzoli, "Properties of the scalar variance transport equation in turbulent channel flow," Phys. Rev. Fluids **4**, 024606 (2019).
[91]MATLAB version 9.8.0.1323502 (R2020a), The Mathworks, Inc., Natick, Massachusetts, 2020.
[92]I. Amidror, "Scattered data interpolation methods for electronic imaging systems: A survey," J. Electron. Imaging **11**, 157–176 (2002).
[93]A. N. Karpetis and R. S. Barlow, "Measurements of flame orientation and scalar dissipation in turbulent partially premixed methane flames," Proc. Combust. Inst. **30**, 665–672 (2005).
[94]H. Zhou, Z. Li, T. Yang, E. R. Hawkes, Z. Ren, H. Wang, and A. Wehrfritz, "An evaluation of gas-phase micro-mixing models with differential mixing timescales in transported PDF simulations of sooting flame DNS," Proc. Combust. Inst. (published online 2020).
[95]R. R. Cao and S. B. Pope, "The influence of chemical mechanisms on PDF calculations of nonpremixed piloted jet flames," Combust. Flame **143**, 450–470 (2005).
[96]C. Schneider, A. Dreizler, J. Janicka, and E. Hassel, "Flow field measurements of stable and locally extinguishing hydrocarbon-fuelled jet flames," Combust. Flame **135**, 185–190 (2003).
[97]L. Cutrone, P. De Palma, G. Pascazio, and M. Napolitano, "A RANS flamelet–progress-variable method for computing reacting flows of real-gas mixtures," Comput. Fluids **39**, 485–498 (2010).
[98]M. Nik, S. Yilmaz, P. Givi, M. Sheikhi, and S. Pope, "Simulation of Sandia flame D using velocity-scalar filtered density function," AIAA J. **48**, 1513–1522 (2010).
[99]M. Sheikhi, T. Drozda, P. Givi, F. Jaberi, and S. Pope, "Large eddy simulation of a turbulent nonpremixed piloted methane jet flame (Sandia flame D)," Proc. Combust. Inst. **30**, 549–556 (2005).
[100]A. Vreman, B. Albrecht, J. Van Oijen, L. D. Goey, and R. Bastiaans, "Premixed and nonpremixed generated manifolds in large-eddy simulation of Sandia flame D and F," Combust. Flame **153**, 394–416 (2008).
[101]S. B. Pope, "Computationally efficient implementation of combustion chemistry using *in situ* adaptive tabulation," Combust. Theory Modell. **1**, 41–63 (1997).
[102]V. R. Katta, L. Goss, and W. M. Roquemore, "Effect of nonunity Lewis number and finite-rate chemistry on the dynamics of a hydrogen-air jet diffusion flame," Combust. Flame **96**, 60–74 (1994).
[103]J. B. Bell, R. K. Cheng, M. S. Day, and I. G. Shepherd, "Numerical simulation of Lewis number effects on lean premixed turbulent flames," Proc. Combust. Inst. **31**, 1309–1317 (2007).
[104]W. Ramaekers, J. Van Oijen, and L. De Goey, "*A priori* testing of flamelet generated manifolds for turbulent partially premixed methane/air flames," Flow, Turbul. Combust. **84**, 439–458 (2010).

© Author(s) 2021